

Connecting Planetary Composition with Formation

Ralph E. Pudritz, Alex J. Cridland, & Matthew Alessi

Abstract The rapid advances in observations of the different populations of exoplanets, the characterization of their host stars and the links to the properties of their planetary systems, the detailed studies of protoplanetary disks, and the experimental study of the interiors and composition of the massive planets in our solar system provide a firm basis for the next big question in planet formation theory. How do the elemental and chemical compositions of planets connect with their formation? The answer to this requires that the various pieces of planet formation theory be linked together in an end-to-end picture that is capable of addressing these large data sets. In this review, we discuss the critical elements of such a picture and how they affect the chemical and elemental make up of forming planets. Important issues here include the initial state of forming and evolving disks, chemical and dust processes within them, the migration of planets and the importance of planet traps, the nature of angular momentum transport processes involving turbulence and/or MHD disk winds, planet formation theory, and advanced treatments of disk astrochemistry. All of these issues affect, and are affected by the chemistry of disks which is driven by X-ray ionization of the host stars. We discuss how these processes lead to a coherent end-to-end model and how this may address the basic question.

Ralph E. Pudritz

Department of Physics and Astronomy, McMaster University, Hamilton, Ontario, Canada, L8S 4E8; Origins Institute, McMaster University, Hamilton, Ontario, Canada, L8S 4E8, e-mail: pudritz@mcmaster.ca

Alex J. Cridland

Leiden Observatory, Leiden University, 2300 RA Leiden, the Netherlands e-mail: cridland@strw.leidenuniv.nl

Matthew Alessi

Department of Physics and Astronomy, McMaster University, Hamilton, Ontario, Canada, L8S 4E8, e-mail: alessimj@mcmaster.ca

Introduction

The remarkable pace of the discovery and characterization of exoplanets over the last 20 years suggests that a comprehensive, empirically verifiable theory of planet formation may now be possible. Planet formation is a complex process involving a series of quite distinct pieces of physics and chemistry on physical scales ranging from micrometers to hundreds of AU. As the other chapters in this section clearly show, each of these links in the long chain leading from planet formation to their observed dynamical, structural, and chemical properties require theoretical solutions to a number of deep problems. While the connection between how planets form and their ultimate physical properties and chemical composition is at present, poorly understood, rapid progress is now being made. There are several general reasons for optimism.

On the observational side, the discovery of over 3000 exoplanets with thousands more to come has revolutionized our understanding of planet formation and properties (Mayor and Queloz 1995; Queloz et al. 2000; Pepe et al. 2004; Udry and Santos 2007; Howard et al. 2010, 2012; Batalha 2014; Bowler 2016). Statistical samples are now large enough that the properties of at least 4 planetary populations (hot and warm Jupiters, mini-Neptunes, and super Earths) can be discerned. We are also starting to link the properties of stars with their planetary systems. There are, compliments of the ALMA revolution, major advances in high resolution and chemical studies of protostellar disks in which planets form. The chemical and physical properties of the outer regions of disks are being probed for a wide range of host stars, and this has already yielded the surprising fact that either low dust/gas ratios or a very large fraction of carbon (a factor of 100) are missing from the gas phase. JWST will tackle the inner regions of disks, as well as the atmospheres of exoplanets. In the solar system, the Juno mission has for the first time, revealed the existence of a core within the planet which may be more dilute than expected. Thus, the physical and chemical processes leading to planet formation as well as the resulting populations can now begin to be studied and tested using a wide variety of ground and space based observatories and probe.

On the theory side, major advances over the last decade include the development of sophisticated theories of planetary migration, dust evolution and the growth of pebbles and planetesimals, a deeper understanding of radiative heating processes, and the rise of astrochemistry as a tool to probe the process of disk evolution and planet formation. All of these advances have been made with the help of a growing arsenal of powerful and sophisticated computer codes. A successful comprehensive theory now requires that it addresses an array of ever more stringent inputs and constraints.

This progress has given rise to a series of important questions. The key question that motivates all aspects of this review is this. Is it possible that despite this plethora of complex processes, is there still a clear thread that connects their composition and other physical properties with their formation? Or have these links been erased as one process takes over from the previous one? If there is such a connection, do chemical abundance patterns of gaseous atmospheres - say the ra-

tio of carbon to oxygen (C/O) abundance - reflect on formation conditions, such as planet formation at ice lines? Are the observed inhomogeneities in disks such as gaps and rings a consequence of planet formation, opacity transitions, other? The transport of angular momentum is central to disk evolution and planet formation so are there imprints of these mechanism(s) left on planetary populations? Given that information about planetary compositions is most likely to come from observations of their atmospheres, to what degree are the bulk characteristics of the interiors of planets linked to the composition of their atmospheres? These are just a few of the interesting questions that arise in understanding this story.

The goal of this review is to outline progress in the connections between planet formation in evolving (dynamically and chemically) disks and the physical and chemical properties of the end product. Most of the analysis addresses processes that occur while planets are forming in their natal disks. We will step along from the basic properties of evolving protostellar disks and planet migration and formation and end up with predictions about populations of planets whose statistical properties that can be confronted with the data. This section of Springer's *Handbook of Exoplanets* contains excellent reviews of various aspects of planet formation, with an overview by Armitage (see also Armitage (2010)). In addition, the reader may also consult a number of recent review articles on the various pieces of this problems including Testi et al. (2014) for disks and dust evolution; Turner et al. (2014) for disks and angular momentum transport; Kley and Nelson (2012) for planet migration, and Raymond et al. (2014), Helled et al. (2014), and Benz et al. (2014) for planet formation.

Observational Constraints

The basic properties of exoplanets can be conveniently summarized in just 4 or 5 important diagrams. The first, and perhaps most fundamental is the mass- semimajor axis (M - a) diagram which can be conveniently divided into three or four planetary populations (Chiang and Laughlin 2013; Hasegawa and Pudritz 2013). The fact that Jovian planets pile up at a characteristic orbital radius of 1 AU, with slightly smaller mass hot Jupiters inside 0.1 AU is good evidence that these massive planets must have moved substantially during their formation in disks (see chapter by Izidoro and Raymond). The theory of planet migration that has arisen to explain this rests on ideas of how planet-gas gravitational interaction and disk angular momentum transport works. The recent discovery of a Hot Jupiter with an estimated mass of $1.66M_{Jup}$ orbiting a young, weak-lined, T-Tauri star Tap 26 - a system that is only 17 Myr (Yu et al. 2017) - at 0.0968 AU has been interpreted as evidence for Type II migration of the planet while in its host disk. This is too little time for planet-planet scattering processes to have taken place.

A second breakthrough are the mass-radius (M - R diagram) relations governing planetary structure that are now being uncovered so that planetary structure and composition can, for the first time, be explored (Howard et al. 2013; Rogers 2014;

Chen and Kipping 2017). An important issue here is that it is the composition of the materials accreted onto forming planets, in particular the overall elemental abundances, plays a major role in determining the radius of a planet for a given mass. This is especially true for low-mass planets, whose radii depend sensitively on whether the planets are rocky, have substantial water contents, or have retained atmospheres. Knowledge of planetary composition will soon be greatly enhanced as JWST and other observatories make precise measurements of the composition of planetary atmospheres.

The third major diagram is the so-called planet-metallicity relation (Fischer and Valenti 2005; Wang and Fischer 2015) which says that massive planets are more likely to be detected around stars only if they have sufficiently high metallicity (solar and above). These authors found that for a limited range of stellar masses (0.7 - 1.2 M_{\odot}) that the probability of a star to host a giant planet scaled as the square of the number of iron atoms; $P_{planet} \propto N_{Fe}^2$. Later studies, carried out for a wider range of stellar masses, found that more massive stars also tend to host Jovian planets, with the scaling $P_{planet} \propto N_{Fe}^{1.2 \pm 0.2} M^{1.0 \pm 0.5}$ (Johnson et al. 2010). The most recent research affirms a strong planet-metallicity relation for Jovian planets while stars of all masses and metallicities host low mass planets. These findings suggest that low mass planets can form in all disks but that only a fraction of these in high metallicity, or in sufficiently massive disks can grow into massive planets within the disk lifetime (Ida and Lin 2005; Hasegawa and Pudritz 2014).

The fourth major diagram is the eccentricity distribution of planets which shows that large eccentricities accrue to a significant number of massive exoplanets. The median value of this eccentricity is very high $\simeq 0.25$. The eccentricity of single massive planets can be attributed to planet-planet scattering interactions after the gas disk has been dispersed (Chatterjee et al. 2008; Jurić and Tremaine 2008).

Another important result is the observed misalignment between the orbital plane of a traversing planet and the equatorial plane of the rotating star measured via the Rossiter-McLaughlin effect (see chapter by Tibaoud). Roughly 1/3 of hot Jupiters show such misalignments. This raises an important question: Did these planets arise through dynamical interactions after migration in the disk had placed them in close-in orbits? Or did they arrive at these innermost orbits by some dynamical process such as the Kozai mechanism coupled with tidal friction?

In the latter case, a distant companion star can cause eccentric motions of a planet whose orbit can shrink and circularize drastically with time due to tidal interaction with the star, leading to close-in Jupiters with high eccentricity (Fabrycky and Tremaine 2007). The observation of a hot Jupiter in orbit around a young T-Tauri star mentioned earlier suggests that at least in some cases, migration in disks can quickly move massive planets into close in orbits, although whether these would be perturbed out of plane would depend on subsequent planet-planet interactions. It may be that the elemental abundances of such planets will ultimately discriminate between planets brought in via disk processes, sampling materials from the inner disk regions, as compared to scattered bodies originally formed in outer disk regions whose compositions reflect the dominance of ices.

Finally, one of the most prominent dynamical features in the M-a diagram are the numerous, extremely compact systems that are well aligned and having short periods (Fang and Margot 2012; Hansen and Murray 2013; Chiang and Laughlin 2013). Although the spacings between orbital pairs seems to be random, nevertheless, there is an abundance of them that are just wide of major mean motion resonances (MMRs) and a lack of such pairs just inside these (Lissauer et al. 2011; Fabrycky et al. 2014). One of the explanations for this behaviour is the effect of planet-planetesimal disk interactions on trapped, resonant pairs of planets (e.g. 2:1) (Chatterjee and Ford 2015). It is clear therefore, that the M-a diagram is a composite recording both the history of planet-disk evolution as well as planet-planet and other dynamical interactions.

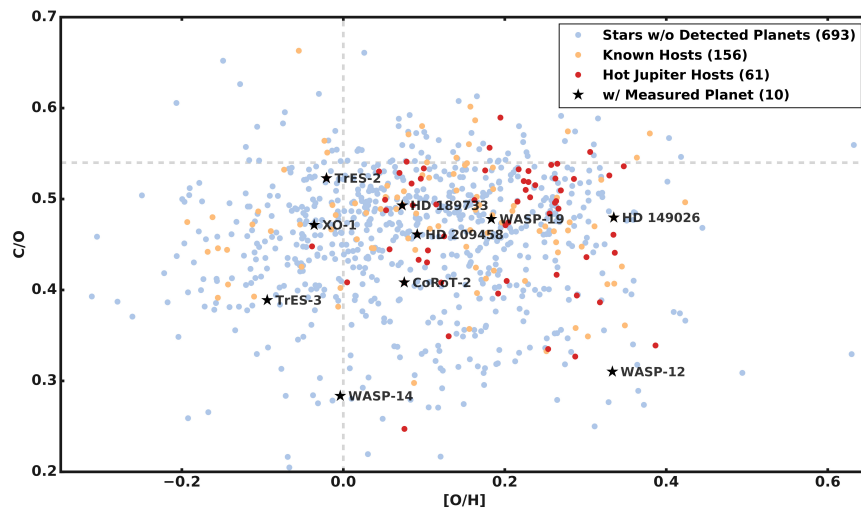
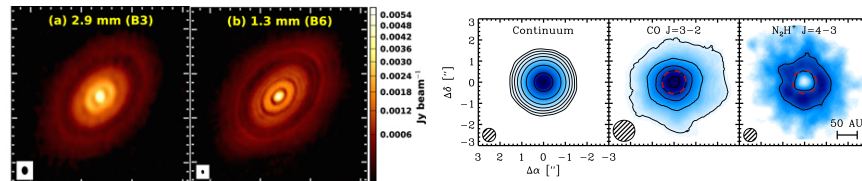


Fig. 1: The distribution of C/O and O/H for a wide range of stars with and without planets. The dotted lines denote the solar values ($C/O = 0.54$). Clearly there is no preference in C/O or O/H in the formation of planets, and particularly for hot Jupiters. Figure from Brewer et al. (2017), AJ, 153, 83. Reproduced with permission ©AAS.

Turning now to the host stars of planetary systems, their chemical composition and radiation fields are essential external inputs for models. Observations of the metallicity distributions and element ratios such as C/O and C/N of stellar atmospheres (Brewer et al. 2017) inform us about the distribution of element abundances in the initial accretion disks out of which both the star and its retinue of planets formed. These materials were accreted onto the planet as it migrated through the disk. Figure 1 shows the C/O and O/H ratios of 693 stars associated with detected planets (eg. Hot Jupiters), indicating that our Sun's C/O ratio is high compared to many planet bearing stars. The figure therefore provides information about the range

of compositions and metallicities of the initial disks that hosted their forming planets. The difference between the composition of Jovian planets, and the host star metallicity, is most readily understood as a consequence of where and how planets accreted most of their gas - indicating the possible role of ice lines as places where planets acquired most of their gas (Öberg et al. (2011b), Madhusudhan et al. (2014), Bergin and Cleeves review). The X-ray luminosities of protostars control the ionization state of their protostellar disks. This is another key external stellar control parameter for planet formation in that the ionization drives disk chemistry, which controls the extent of so-called dead zones in disks (regions free of turbulence driven by magnetic instabilities). The UV irradiation of stars also controls the disk lifetimes due to photoevaporation processes (Gorti et al. 2016).

Surveys will increasingly inform us about the distribution of protostellar disk masses and their lifetimes (Haisch et al. 2001; Hernández et al. 2007; Hartmann 2008; Andrews et al. 2010). The distribution of disk masses is related to the initial conditions for disk formation and arise from the range of dense core masses and their level of magnetic braking and internal turbulence that will shape their collapse into protostellar disks (eg. Seifried et al. (2015), review by Li et al. (2014)). The distribution of disk lifetimes is related to a combination of the processes that carry of disk angular momentum (turbulence, disk winds, or spiral waves) as well as by disk photoevaporation processes that will ultimately dissipate them. There is growing understanding of how dust evolves in disks and of the changes in chemical composition as a function of disk radius, arising from the appearance of various opacity transitions and ice-lines (see Chapters by Bergin and Cleeves, Andrews and Birnstiel).



(a) High resolution imaging of the HL Tau disk at mm-wavelengths. The resolution afforded by ALMA has given us an impressive look at the structure of protoplanetary disks. Figure from ALMA Partnership et al. (2015), *ApJ*, 808, L3. Reproduced with permission ©AAS.

(b) Detection of the CO ice line in the TW Hya disk. The position of the CO ice line is indicated by the inner gap of the N₂H⁺ emission because it can be easily destroyed by gaseous CO. Figure from Qi et al. (2013), *Science*, 341, 630. Reproduced with permission ©AAAS.

Fig. 2: Examples of observational studies of the physical and chemical structure of protoplanetary disks.

One of the great observational surprises from ALMA is that disks have turned out to be far from the smoothly varying structures pictured in highly idealized theoretical models for accretion disks for decades. ALMA observations as an example,

show that disks host a large number of symmetric ring and gap structures, as well as asymmetric structure such as spiral waves and lopsided dust distributions revealing that density and temperature inhomogeneities dominate. It is not yet clear whether these structures are the consequence of disk physics, or the result of planet formation. Dust also has significant radial drift with respect to the gas in disks. Figure 2a shows the now famous image of HL Tau with its series of either 5 (Tamayo et al. 2015), or 3 (Zhang et al. 2015) gaps, whose origin has a variety of possible explanations ranging from the appearance of various ice lines (opacity transitions) to the perturbing influence of planets that are carving out gaps or creating pressure bumps into which dust gathers. In Figure 2b, we see observational evidence for the existence of the CO ice line in TW Hya. These inhomogeneities have important implications for planet formation in that they can give rise to dynamical traps for migrating low mass planets, as well as traps for rapidly moving dust. Finally, observations of debris disks are telling us about the degree to which carbon was frozen out and stored in planetesimals. These can retain imprints of planet formation and disk chemistry processes (see chapter by Wyatt).

In short, there is now a wealth of statistical data on properties of stars, exoplanets, and protoplanetary disks that can be brought to bear on constructing a comprehensive picture of planet formation.

Physical and chemical components of an end-to-end model

The pioneering steps towards connecting the data in M-a diagram with a statistical treatment for planet formation in a core accretion model were taken in the first population synthesis paper of Ida and Lin (2004a). The intent of this approach was to model the evolution of planets in the M-a diagram using planet formation theory coupled to a statistical treatment of the initial conditions - the primary one being the distribution of disk masses. Differences between predicted and observed populations then offer insight into how theory needs to be further developed (Benz et al. 2014). This is perhaps the most important first way that theory could be tested given that; (i) only the initial conditions (eg. disks distributions) and final results (planetary systems in M-a) diagram are directly observed and that planet formation is not (yet), and (ii) the diversity of planetary properties arises in part from distributions of initial controlling parameters (eg. disk masses, metallicities, ionization rates, etc.). This work was followed up for stars of different metallicity and masses (Ida and Lin 2004b, 2005). These were then improved by more comprehensive treatments of various migration processes including an analysis of what is needed to slow rapid migration (Ida and Lin 2008a), and an examination of the ability of the ice line to act as a potential migration trap (Ida and Lin 2008b). Investigations of the effects of stellar masses on planet populations were carried out by Alibert et al. (2011).

The basic components of an end-to-end theory of planet formation that also includes the chemical composition of newly formed can be briefly summarized.

- (i) Adopt a model for the structure and evolution of protostellar disks, from the initial conditions (reflecting their formation), through disk evolution due to the proposed mechanism of angular momentum transport, to the end phases in which photo evaporation of disks leads to their rather quick demise 3 - 10 Myr after their formation. The majority of treatments of angular momentum transport in disks assume that disks are turbulent, and that therefore it is “turbulent viscosity” that transports angular momentum (Shakura and Sunyaev 1973; Lynden-Bell and Pringle 1974), the source of the turbulence being the magneto-rotational instability (MRI) (Balbus and Hawley 1991). It has long been known however, that for ideal MHD, magneto-centrifugal disk winds can be more effective than even turbulence in transporting away disk angular momentum (Blandford and Payne 1982; Pudritz and Norman 1986; Pelletier and Pudritz 1992; Pudritz et al. 2007). Recent breakthroughs in non-ideal MHD effects in disks show that MRI turbulence may be entirely suppressed in the central, planet forming zones of disks (≤ 10 AU) leaving only an MHD disk wind to transport out the angular momentum (Bai and Stone 2013; Gressel et al. 2015). The wind picture of angular momentum transport may have profound consequences for planet formation and migration (see Nelson’s chapter). Finally, disks are likely to be self-gravitating in their early stages of formation, and therefore spiral waves will appear which can be highly effective in transporting disk angular momentum radially (Li et al. 2014).

- (ii) Prescribe the evolution of solids within such disks. Dust may arrive in the disk during disk formation by the collapse of an initial protostellar core, or form as the result of a condensation sequence wherein minerals appear at different disk radii depending on their condensation temperatures. Subsequent dust settling into the midplane leads to rapid coagulation. Dust grains will grow due to agglomeration near the disk midplane, while at the same time undergoing radial drift due to drag forces. Radial drift changes the dust to gas ratio throughout the disk and will help dictate where planets may form (see chapter by Andrews and Birnstiel).

- (iii) All planets, whether terrestrial, or massive, start by the accretion of solids into smaller mass embryos and cores. The nature of solid accretion could reflect either collisions of planetesimals to build oligarchs, pebble accretion onto rapidly growing bodies, or a combination of these. The composition of these materials will play a basic role in determining the M-R relation.

- (iv) Migration of embryos and forming planets. Theories of migration for bodies with masses that are too small to open gaps (Type I migration) focus on two kinds of torques due to planet-disk interaction: wave torques due to Linblad resonances at some distance (a few Hill radii) from the forming planet (usually resulting in inward migration) and co-rotation torques exerted by gas orbiting very close to the forming planet, generally resulting in outward migration. Real disks also have inhomogeneities in temperature and densities, and these prove to be crucial in providing zones of “zero net torque” or planet traps.

- (v) Gas accretion onto massive cores leading to accretion runaways that quickly build Jovian planets. The composition of gas accreted during this phase will determine a great deal about the properties of the Jovian atmospheres (see chapter by D’Angelo and Lissauer). The latter is best followed using time dependent gas chem-

istry codes (Fogel et al. 2011; Helling et al. 2014; Cridland et al. 2016; Eistrup et al. 2016).

- (vi) Gap opening, Type II migration, and the end of accretion from the disk. The late accretion from planetesimals may affect the chemical composition of the atmospheres.

- (vii) End of planet- gas disk interaction that arises from the photo evaporation of the disk. This does not yet mark end of planetary chemical enrichment of atmospheres.

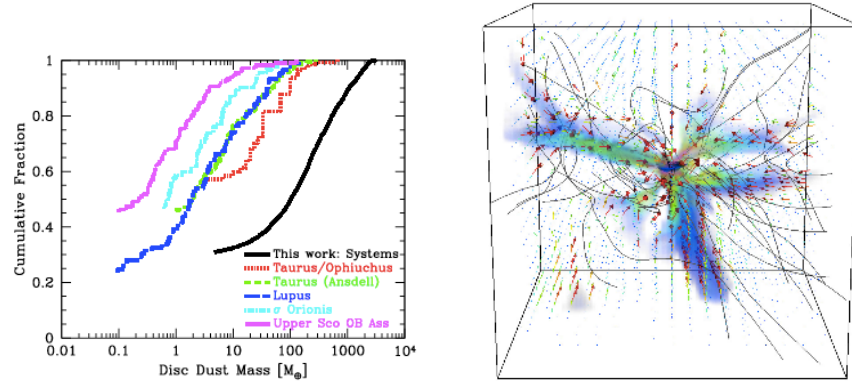
- (viii) The dynamical evolution of the gas-free planetary system in which planet-planet interactions will rapidly lead to high eccentricities, the loss of mean motion resonances, and probably the loss of some planets (chapter by Morbidelli). The scattering of planetesimals onto colliding trajectories with gas giants may lead to considerable metal enrichment in Jovian atmospheres.

- (ix) The structure of a planetary atmosphere depends on its pressure-temperature (P-T) profile as well as its chemical composition. For massive planets, this is usually computed using chemical equilibrium models based on the elemental abundances of gas and solid materials delivered to the forming atmosphere during its formation (eg. see Madhusudhan chapter). For Super Earths, the composition of secondary atmosphere that forms due to outgassing will depend on the accretion history as well, as volatiles undergo outgassing from the newly formed planet.

Disk formation and initial chemical composition

Disks with radii > 30 AU have now been observed during the earliest phases of protostellar evolution - the Class 0 and Class I sources. (eg. Tobin et al. (2015) - class 0; Andrews and Birnstiel chapter). Given that the star forming cores within filamentary molecular clouds have a wide range of masses and angular momenta, one expects a wide range in protostellar disk properties.

Recently, Bate (2012) published the highest resolution (down to the opacity limit for fragmentation - a few Jupiter masses), radiation hydrodynamics simulation of a forming star cluster. The initial low mass, cluster forming clump ($500 M_{\odot}$) had an initial radius of 0.40 pc and temperature of 10^4 K. The resulting initial mass function of the stars closely followed the observations (Chabrier 2005). A comprehensive study of the properties of disks formed in this simulation have now also been published (Bate 2018). The disks show an enormous diversity in types and sizes. Systems can be formed by a wide range of processes including filament fragmentation, disk fragmentation, dynamical processing, accretion and ram pressure stripping. Disk morphologies include warped and eccentric disks. Disk masses increase until 10^4 yrs with masses up to $0.5 M_{\odot}$. Disk masses range from M_d/M_{\odot} 0.1 – 2 for times $\leq 10^4$ yrs, after which they decline. Thus, disk masses at these early times are some 30 - 300 times more massive than they are during the Class II phase (when they are ~ 1 Myr old). The surface density profiles are flatter than the Minimum Mass Solar Nebula, with $\Sigma_d \propto r^{-1}$, rather than the classic MMSN $r^{-3/2}$



(a) Cumulative mass distribution of protoplanetary disks. The disks produced in the numerical simulations of Bate (2018) (black line) tend to be more massive than the observed systems because they are much younger than the observed systems. Figure from Bate (2018), MNRAS, 475, 5618. Reproduced with permission ©Oxford University Press.

(b) Three-dimension snapshot from an MHD collapse calculation for the collapse of a 2.6 solar mass core. Black lines are magnetic field lines, blue coloration is of dense filaments bringing gas into the disk forming in the central region. The scale of the box is 1300 AU. Figure reproduced from Seifried et al. (2015), MNRAS, 446, 2776.

Fig. 3: Left: Cumulative mass distribution for disks in radiative hydrodynamics simulations. Right: Image of a disk forming in a turbulent MHD simulation

These radiation hydrodynamics simulations did not include magnetic fields. A reasonably strong magnetic field will strongly brake smooth, rotating clouds so that only very small disks can form - a result known as the “magnetic braking problem”. This can be resolved in turbulent simulations in which the magnetic torques are much reduced, leading to larger disks more resembling the hydrodynamic results (Li et al. 2014; Seifried et al. 2015).

The left panel of Figure 3 shows the cumulative distribution of disk masses in Bate’s (2018) turbulent radiative hydrodynamics simulation (figure 3a). The distribution is roughly an order of magnitude more massive than observed disks in various clouds - seen at much later times. It is not clear how to connect the time of the simulation with the time in the observed clouds, but the latter pertains to objects much older than the newly collapsed disks in the simulation. The right panel of the figure shows an image of a forming disk in a turbulent MHD simulation (Seifried et al. 2015) (figure 3b). Here too one sees a highly filamentary collapse process in which 5 or so filaments bring material to the forming disk while MHD torques are inefficient in providing a magnetic brake at this earliest phase. More generally, collapsing, magnetized cores will launch magnetically driven outflows and winds as the disks are forming, and long before the final process of stellar assembly is complete

(Banerjee and Pudritz 2006; Li et al. 2014). Thus, even in the earliest stages, MHD disk winds will play an important role in the angular momentum evolution of these systems, and this can lead to profound effects on planet formation.

The dust and chemical composition of the protostellar core can, to some degree, be inherited by the disk. Thus, whereas the largest part of dust growth will occur at the disk mid plane because coagulation is more rapid in high density environments, coagulation helped by ice coated mantles (eg. Ormel et al. (2009)), grows grains to several microns at core densities of 10^5 within ~ 1 Myr. Dust can grow up to \sim mm sizes within the infalling envelopes (e.g. Jørgensen et al. (2009)).

Chemical processing also occurs within the dense gas of star forming cores. In prestellar cores, the most abundant phase for molecules with elements heavier than hydrogen and helium is a solid. It has been known for over 40 years (Gillett and Forrest 1973) that infrared absorption of interstellar ices gives us a glimpse into the chemical composition of star forming material. Water and CO ice were the first to be discovered, and represent the most abundant molecules after H_2 . They are followed closely in abundance by CO_2 which was not found until the launch of IRAS because of strong absorption in the atmosphere (Öberg et al. 2011b). With newer space-based studies by ISO and Spitzer, larger, more complex hydrocarbons have been inferred in the infrared absorption of ices towards star forming regions (Öberg et al. 2011a). The formation of these hydrocarbons through the hydrogenation of frozen CO has been studied both theoretically (Walsh et al. 2014; Vasyunin et al. 2017), and in laboratory experiments (Butscher et al. 2015; Chuang et al. 2018), and represents the first steps towards pre-biotic chemistry. With the latest generation of telescopes these pre-biotic molecules have begun to be found around both young stars (Jørgensen et al. 2012), and in prestellar cores (Ligterink et al. 2017; Rivilla et al. 2017).

Whether these species survive to the protoplanetary disk is still debated. There are two primary pictures for the delivery of element from the prestellar core to the disk: ‘inheritance’ and ‘reset’. In the inheritance scenario all molecular species that were formed in the prestellar core are delivered to the disk intact, while in the reset scenario there is a thermal event that breaks all molecules down to their base elements (Pontoppidan et al. 2014). As an example, detailed chemical studies of over 39 different molecules, grouped into 4 families of related molecules, have been carried out in the well studied, pre-stellar core L1544, indicate that significant differentiation of C and N bearing molecules occurs. Such studies holds great promise for understanding the initial chemical conditions before disks formed (Spezzano et al. 2017). Deuterated water could be a good tracer of these different process because its enrichment is favoured in cold, ionized environments like prestellar cores (eg. L1544), and in a protoplanetary disk at large radii (Cleeves et al. 2014). In the inheritance scenario the deuteration of water would be homogeneous across the disk, while in the reset scenario there would be a deuterium gradient. Of course the true answer may be somewhere between these two extremes. Carbon deficiency in the solids throughout the solar system could be evidence of reset in the inner solar system, and inheritance in the outer solar system. The number of carbon atoms relative to silicon on the Earth is under abundant by four orders of magnitude relative the

ISM while comets like Halley are not similarly underabundant (Bergin et al. 2015). This could be evidence of thermal processing of material because while carbon generally exists in the solid phase in prestellar cores (Bergin et al. 2015) if the grains are destroyed upon reaching the disk, the carbon would not re-condense as a solid in the inner solar system (Pignatale et al. 2011).

Disks: structure, evolution, and chemistry

As the inflow of gas onto the forming disk comes to an end, the earliest stage of disk evolution has the disk mass being comparable to that of the protostar (Seifried et al. 2015; Klassen et al. 2016; Bate 2018). The self gravity of the disk, measured by the Toomre Q parameter ($Q = c_s \Omega / 4\pi G \Sigma$ where c_s is the sound speed, Ω is the local angular velocity of the disk, and Σ is its surface density), is significant ($Q \simeq 1$ (Kratte et al. 2008)). In the first 10^5 yrs, the system evolves from the Class 0 to the Class I state in which outflows are the most powerful. Angular momentum transport in the disk arises from spiral waves (due to the gravitational instability of the disk launched when $Q \leq 1$), together with disk winds and turbulence. It is during this time that the first stages of planetesimal formation would have already taken place.

The subsequent phase of disk evolution in the much better studied Class II systems, involves thin, Keplerian disks that are in vertical hydrostatic balance. The vertically averaged angular momentum equation that governs a disk undergoing a total stress σ is (Pudritz and Norman 1986; Turner et al. 2014; Bai 2016),

$$\dot{M}_a \frac{d}{dr}(ru_\phi) = \frac{d}{dr}(2\pi r^2 \langle \sigma_{r,\phi} \rangle) + 2\pi r^2 \sigma_{z,\phi}|_{-h}^{+h} \quad (1)$$

where the accretion rate is $\dot{M}_a = 2\pi r \Sigma v_r$ for a radial inflow speed of the gas v_r , and the angle brackets in the first term indicate taking the vertical average of the torque by integrating over z . The total stress has contributions from both turbulence, and the Maxwell stress of threading magnetic fields. The first term on the right hand side denotes angular momentum flow in the radial direction, while the second term is angular momentum flow out in the vertical direction due to wind torques. In the case of shear turbulence, the stress is the average of the turbulent fluctuations, $\sigma_{r,\phi} = -\rho \delta v_r \delta v_\phi$. In the presence of a toroidal magnetic field B_ϕ in the disk, a radial field B_r can also contribute to flow in the radial direction through the Maxwell stress component; $\sigma_{r,\phi} = B_r B_\phi$. This possibility arises in recent models of non-ideal MHD wherein the Hall effect can produce an instability leading to a radial field component (eg. (Bai 2014; Lesur et al. 2014; McNally et al. 2017)). A threading vertical component of the field B_z however, exerts a torque on the disk with $\sigma_{z,\phi} = B_z B_\phi$ leading to an MHD disk wind, which is central to the action of the ubiquitous jets and outflows that accompany the formation of all young stars, regardless of their mass (Frank et al. 2014; Ray et al. 2007; Pudritz et al. 2007).

Physical models of accretion disks have focused heavily on the assumption that angular momentum is transported by turbulent viscosity, first addressed in the

seminal papers by Shakura and Sunyaev (1973), Lynden-Bell and Pringle (1974). Here, the turbulence arises from the shearing Keplerian flow and takes the form $\sigma_{r,\phi} = \nu \Sigma r d\Omega/dr$. The effective viscosity of the disk ν can then be shown to scale with the disk scale height as $\nu = \alpha c_s h$ with the famous α parameter. Steady state disks then have a radial accretion rate \dot{M}_a , which, away from the inner boundary of the disk can be written as

$$\dot{M}_a = 3\pi\nu\Sigma = \text{const} \quad (2)$$

In order to drive an accretion flow at the rate observed to fall onto T-Tauris stars, $\alpha_{SS} \simeq 10^{-2} - 10^{-3}$. The angular momentum is carried out radially leading to the slow, outward radial spreading of the disk from its initial state. The energy that is available to drive the turbulence is given by the gravitational potential energy release across each annulus of the disk, which is dissipated as heat and radiated away. Assuming that each annulus of the disk radiates as a black body then one readily derives that viscous heating results in an effective temperature of the disk $\sigma T_{eff}^4 = (3/8\pi)\dot{M}_a\Omega^2$ and thus the scaling: $T_{eff}(r) \propto \dot{M}_a^{1/4} r^{-3/4}$.

The second source of heating is the radiation field of the central star. A flaring disk will intercept flux from the star, and will be absorbed by the dust and re-emitted at IR wavelengths in the disk's surface layer. Assuming this is a black-body process, the temperature then has a shallower fall off with disk radius $T(r) \propto r^{-1/2}$ (Hartmann and Kenyon 1987). This can be extended by considering that only the surface layers of the disk are directly heated by the star while the deeper parts of the disk are heated by radiation re-emitted from it, which are solved in concert with hydrostatic balance that produces a flaring disk. The result is a surface temperature that scales as $T_{surf} \propto r^{-2/5}$ while for the interior $T \propto r^{-3/7}$ for disk radii $r \leq 84AU$ (Chiang and Goldreich 1997). Observations indeed show that the temperature distribution arising from viscosity are too steep to explain the mm and submm observations of disks, having an average temperature exponent $T \propto r^{-q}$, where for the dust, $q_{dust} \simeq 0.5$ (Andrews and Williams 2007). The temperature of the gas, as determined by CO and [CII] line observations, has a steeper radial decline with $q_{gas} \simeq 0.85$. Since the temperature profiles of dust and gas should be similar on the disk mid plane, the difference here suggests a decoupling of gas and dust at high scale heights above the disk (Fedele et al. 2013).

Unlike viscous heating, radiative heating from the central stars creates a hot surface layer on the disk atmosphere, and a much cooler midplane. This has several important consequences for disk chemistry and dynamics in that the snow-lines for various species are 2-D surfaces that move outward in radius as one moves away from the disk midplane (see chapter by Bergin and Cleeves). The disk radius at which the dominant heating mechanism of the disk transitions from viscous to radiative heating is called the "heat transition" (eg. Lyra et al. (2010); Hasegawa and Pudritz (2011)), which we will denote r_{HT} .

Disks are not static structures and their time evolution due to the long term action of disk viscosity is well known. In general, this is determined by solving the continuity equation for the surface density of the disk, together with the disk angu-

lar momentum equation. For disks driven by purely viscous torques, the equation describing the evolving surface density profile $\Sigma(r,t)$ of a protoplanetary disk becomes:

$$\frac{\partial \Sigma}{\partial t} = \frac{3}{r} \frac{\partial}{\partial r} \left[r^{1/2} \frac{\partial}{\partial r} (r^{1/2} \nu \Sigma) \right]. \quad (3)$$

This diffusion equation describes accretion as the result of a diffuse process driven by the turbulence.

Since the surface density evolves with time, the accretion rate \dot{M}_a must also be affected, and in fact decreases with time. The disk will also lose mass due to photoevaporative processes that are driven by X-ray and UV radiation from the star. The combined effects of accretion and photo evaporation can be combined in a single, time dependent equation for the evolution of the disk's accretion rate (Pascucci and Sterzik 2009; Owen et al. 2011);

$$\dot{M}(t) = \frac{\dot{M}_0}{(1 + t/\tau_{\text{vis}})^{19/16}} \exp\left(-\frac{t - \tau_{\text{int}}}{t_{\text{LT}}}\right), \quad (4)$$

which includes a viscous evolution term multiplied by an exponentially-decreasing photoevaporation factor. In equation 4, τ_{vis} is the disk's viscous timescale, \dot{M}_0 is the accretion rate at the initial time $\tau_{\text{int}} = 10^5$ years, and t_{LT} is the disk's lifetime (Alessi et al. 2017). In this equation the contribution due to viscous diffusion arises from the analytical model by Chambers (2009) for the evolution of a viscous, irradiated disk. The exponential factor is due to rapid photoevaporative truncation of the disk as modelled by Hasegawa and Pudritz (2013) who showed that without a sharp cutoff of viscous evolution planets undergo too much migration and accretion to be able to match the distributions in the M-a diagram. We note that other authors have used different expressions for cut-offs, such as a finite time cutoff to zero (Ruden 2004).

We see that the distribution of disk lifetimes t_{LT} directly impacts the accretion histories of disks and stars through sharp photoevaporation driven cutoffs of the disk surface density. Thus planet-disk interaction ceases fairly quickly once photoevaporation sets in and planets cease their migration. There is another crucial aspect of evolving radiatively heated disks. Since the temperature of the inner viscously heated part of the disk must decline with time (since $T_{\text{visc}} \propto \dot{M}_a^{1/4}$), the heat transition radius r_{HT} moves inwards with time as well. The heat transition radius turns out to also play the role of a planet trap - wherein fast moving low mass planets underling Type I migration are trapped at a point of zero-net torque. We discuss this below. The viscous evolution picture of disks requires an explanation of how turbulence can be excited and maintained in disks. Hydrodynamic Keplerian disks are highly stable to various kinds of perturbations but there is a large literature on how turbulence could be excited. The central pillar on which most thinking about turbulence in disks rests has been the magneto-rotational instability (MRI). In his magisterial treatment of instabilities in magnetized rotating fluids, Chandrasekhar (*Hydrodynamic and Hydromagnetic Stability*, 1960) notes a striking fact about the stability of so-called Couette flows (fluid flow between two rotating cylinders) . For

purely hydrodynamic systems, the well known Rayleigh criterion for fluid stability dictates that the specific angular momentum (i.e., angular momentum per unit mass, $j = v_\phi r = \Omega r^2$) should increase with radius for stable hydrodynamic flows. However, if one threads a rotating Couette flow with a magnetic field, this criterion is profoundly changed: stability requires that Ω must be an increasing function of radius - even in the limit of vanishing magnetic field strength. The seminal paper by Balbus and Hawley (1991), in working on the stability of magnetized accretion disks, rediscovered this result. In the astrophysical context, there is no system that we know of, with the exception of small boundary layer regions, whose angular velocity decreases increases with radius (eg. galactic rotation curves $\Omega \propto r^{-1}$, Keplerian disks $\Omega \propto r^{-3/2}$). Accretion disks, it follows, should be highly unstable to MRI. Growth rates for the most unstable modes in a thin disk are $3/4\Omega$ (Balbus and Hawley 1991) with a vertical wavelength $\lambda_z = 2\pi v_A / \Omega$ where $v_A = B_z / (4\pi\rho)^{1/2}$ is the Alfvén speed in the magnetized gas. If a toroidal field component is also present, then the field becomes buoyant for a plasma "beta" parameter (the ratio of thermal to magnetic pressure in the gas $= 8\pi\rho c_s^2 / B^2$) for sufficiently strong fields $\beta \leq 10$ (Terquem and Papaloizou 1996) and rises out of the disk into the disk corona.

The high column densities of protoplanetary disks prevent much radiation from penetrating the disk, leaving it poorly ionized at the midplane. Thus non-ideal MHD processes such as Ohmic losses, ambipolar diffusion, and the hitherto little investigated Hall effect, all take their toll on the coupling of magnetic fields to gas. The region in the disk where these non-ideal effects conspire to reduce or eliminate the MRI instability is known as the dead zone (Gammie 1996).

Disk evolution in these regions are essentially dead to MRI turbulence, and while very low level turbulence may still be excited by various hydrothermal instabilities (Flock et al. 2012), in the presence of a weak threading vertical field, angular momentum is driven primarily by a disk wind from a largely laminar disk (Bai and Stone 2013; Gressel et al. 2015). The wind is launched from a thin, highly ionized region on the disk surface. Radial flow is possible in such laminar disks if the Hall effect is radial, laminar transport of angular momentum occurs. One of the most distinct aspects of the Hall effects is that the direction of transport of the magnetic flux in disks depends on the polarity of the threading poloidal field component \mathbf{B}_p with respect to the disk rotation axis. If its direction is parallel to Ω , then flux transport is inwards, and if anti-aligned, outwards (Bai and Stone 2017). Since the flux distribution affects the strength of the wind torques, these Hall effects could be significant for the physics of Type I migration. In all situations, it appears that disks do not support MRI turbulence out to distances of 10 AU for standard conditions. This dead zone radius r_{DZ} must evolve with time as the disk thins out.

Disk ionization, turbulence, and angular momentum transport

The ionization of the disk by stellar X-rays, external cosmic rays, and the decay of radionuclides mixed in with the gas plays a central role in the coupling of the mag-

netic field - and hence the genesis of MRI turbulence - to the disk. Disk chemistry is also primarily driven by ionization processes (see Chapter by Bergin and Cleeves). Thus, disk chemistry and angular momentum transport are highly coupled, and as we will see, should therefore be connected to the ultimate element compositions of forming planets.

Non-ideal MHD effects arise from the finite diffusivity of fields in the background gas. Ionization fractions are highest at the disk surface and decrease with increasing optical depth as one penetrates down to the disk mid plane. Thus UV and X-rays are absorbed at column densities of 0.01 and 10 g cm^{-3} respectively. The greatest penetration can be achieved by cosmic rays (CR) which are attenuated by column densities of 100 g cm^{-3} (Umebayashi and Nakano 2009). Unlike X-rays however, CR can be scattered by MHD turbulence. By decomposing MHD perturbations into their three basic modes (slow, Alfvénic, and fast), it has recently been shown that gyroresonance with the fast modes (sound waves compressing the magnetic field) is the dominant scattering process (Yan and Lazarian 2002). This is expected to occur for CR propagation through protostellar and disk winds, as is evidenced by the lack of CR driven chemistry in protostellar disks (Cleeves et al. 2013).

As one moves from the surface to ever greater densities approaching the disk mid plane, first dust grains, then ions, and finally the electrons decouple from the magnetic field. The degree of coupling is measured by three different magnetic diffusivities (Salmeron and Wardle 2003); ambipolar diffusion in the surface low density regions where ions and electrons are well coupled (η_A), the Hall effect at intermediate densities where the ions are decoupled from the fields through insufficient collisions with the neutrals (η_H), and at the greatest depths and densities Ohmic diffusion where even the electrons become decoupled (η_O). While both ambipolar and Ohmic effects behave like diffusive processes, the Hall effect is different in principle. It drives the field lines in the direction of the current density with a tendency to twist that can give rise to non diffusive dynamical processes, such as the generation of a toroidal field from a radial component.

The diffusivities depend upon the ionization of the disk, and it is here that models of disk ionization driven chemistry can play a key role. As an example, the Ohmic diffusivity depends on the electron fraction x_e and disk temperature as $\eta = 234T^{1/2}/x_e \text{ cm}^2 \text{ s}^{-1}$. As one moves towards the disk mid plane, the Ohmic diffusivity grows as the X-rays are screened. Similarly, as the disk evolves, the column density at any radius decreases with time, shifting the region of Ohmic dominance inwards allowing turbulence to appear. The temperature at the disk mid plane, where planetary materials are gathering, is related to the effective temperature of the disk as $T_{mid} = (3\tau/4)^{1/4}T_{eff}$ where $\tau = \kappa_o\Sigma/2$ is the optical depth and κ_o is the disk's opacity. Chemistry codes that can follow disk ionization with time are therefore essential (eg. Cridland et al. (2016, 2017a)).

The damping of MRI instabilities can be measured by the ratio of the growth rates to the damping rates predicted by these diffusivities. These are the so-called Elsässer numbers for each effect: $A_m = v_A^2/(\eta_A\Omega)$, $\Lambda_H = v_A^2/(\eta_H\Omega)$, and $\Lambda_O = v_A^2/(\eta_O\Omega)$. Damping of the turbulence will occur if these numbers take a values of typically

less unity (see Turner et al. (2014) for a review). In the case of Ohmic diffusion, this comparison of damping and growth rates can also be expressed in terms of a comparison of physical scales, namely, that the diffusion will erase fluctuations on a scale smaller than η/v_A , while the fastest growing mode in the disk has a wavelength of $2\pi v_A/\Omega$.

The appearance of a dead zone in disks has important implications for planet formation and chemistry. In order to maintain a constant accretion rate throughout the radial structure of a disk at any time, the relative roles of turbulence and disk winds in transporting angular momentum must change as one moves from the outer, well ionized regions of the disk, into the region of the dead zone, where MRI turbulence will be damped and the bulk of the angular momentum flow is contingent on wind, and or Hall term transfer. Disk winds do not physically act like turbulent viscosity - the disk does not spread radially outward under the action of a wind but is advocated inwards. Nevertheless, for modelling purposes, it is useful to consider an effective alpha parameter that characterizes the magnitude of angular momentum transport out of the disk by an MHD wind. If we designate an effective α_{eff} parameter for the disk, then one may write $\alpha_{eff} = \alpha_{SS} + \alpha_{wind}$, such that within the disk's dead zone $\alpha_{eff} \simeq \alpha_{wind}$. The existence of a dead zone, expected from the basic physics of disk ionization and the MRI instability, suggests that dust may more rapidly settle to the mid plane within r_{DZ} . Values of α_{SS} may drop to values lower than 10^{-4} in such regions.

Chemistry of evolving disks

Gas

As the disk evolves, its changing physical structure is imprinted on its evolving chemistry. Of principle importance is the reduction of gas temperature and increasing ionization as the disk accretion rate decreases. Because reactions between ions and neutrals lack an activation barrier, the ionization rate plays an important role in dictating the rate of reaction for many gas phase reactions (Eistrup et al. 2016). As the disk surface density drops, and ionizing radiation can more easily penetrate to deeper regions of the disk, driving the chemical system to a (mathematically) steady state - where molecular abundances no longer change with time - more quickly. This steady state differs from the thermodynamic equilibrium solution for a set of reactions, whose final molecular abundances are dictated by Gibbs free energy minimization in that steady states are not necessarily global minima for the Gibbs free energy.

Generally speaking, the gas changes its chemical structure through only a few chemical pathways. They are: freeze out onto and sublimation off of grain surfaces, neutral-ion gas phase reactions, neutral-neutral reactions on grain surfaces, and neutral-neutral gas phase reactions. The rates of each of these reaction path-

ways sensitively depend on the temperature, density, and ionizing flux of the disk's gas.

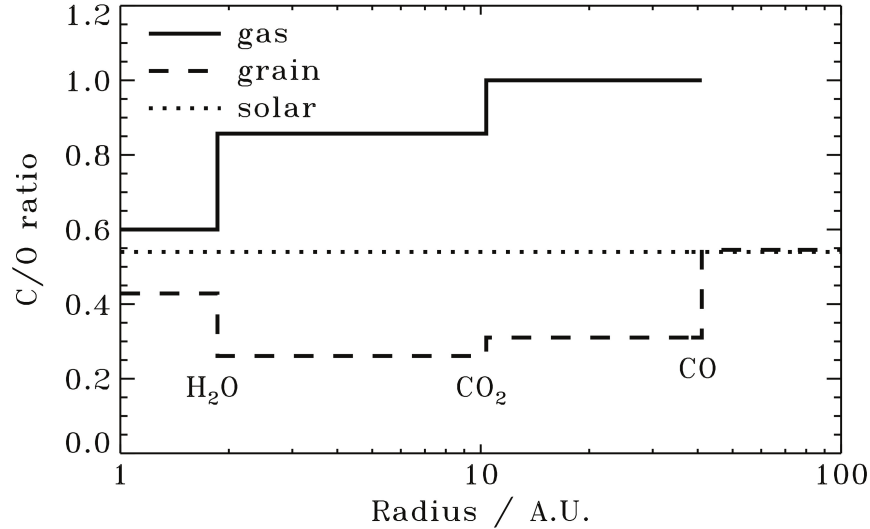


Fig. 4: The distribution of carbon and oxygen through a protoplanetary disk as shown by the carbon-to-oxygen ratio (C/O). The major jumps of C/O result from the freeze out of volatile H₂O, CO₂, and CO at their respective ice lines. Figure from Öberg et al. (2011), ApJ, 743, L16. Reproduced with permission ©AAS.

Figure 4 (from Öberg et al. (2011b)) illustrates a well known, elegantly simple model of the elemental distribution through a disk. It shows the ratio of the total carbon and total oxygen elements (counting the most abundant molecules), known as the ‘carbon-to-oxygen ratio’ (C/O), for gases and solids. At the ice lines of H₂O, CO₂ and CO, C/O changes as particular volatiles freezes onto dust grains. This process is dependent on the local gas temperature, so as the temperature of the gas cools the location of the ice lines (and their jumps in C/O) will move inward. In this model, the only chemical process that is taken into account is the freeze out of volatiles onto grains, which is balanced by their sublimation. In reality once a gas species has frozen onto a grain, it can be chemically processed while in the ice phase. This can be particularly important for the production of molecules like methanol which is produced through the hydrogenation of frozen CO (Walsh et al. 2014).

While these surface reactions will not generally change the C/O of the ices, gas phase reactions can have an impact on both the gas and solid C/O depending on where the reaction occurs. For example, CO has an exceptionally low freeze out temperature (~ 20 K), and hence stays in the gas phase over a wide range of radii (< 40 AU, depending on the disk model). In its gas phase, it will most readily react

with ions like He^+ . This reaction results in its dissociation, leading to an ionized carbon atom, an oxygen atom, and a neutralized helium atom. The oxygen atom will quickly react with H_2 into water and freeze out onto the grains if the reaction occurs beyond the water ice line. The ionized carbon will also react with H_2 to produce CH^+ , then through successive reaction with H_2 react into CH_4 which, if the reaction occurs outside of the methane ice line, will freeze out onto the grains (Walsh et al. 2015). Since the products of this route of CO destruction have different freeze out temperatures (CH_4 being lower than H_2O) the resulting C/O in both the gas and ice will be different depending on the radii where the reaction occurs. The rate of these reactions critically depend on the local ionization rate and temperature of the gas, hence their chemical evolution must be calculated in conjunction with the physical evolution of the disk.

It is particularly important to constrain the possible outcomes of chemical evolution because of its link to the way we interpret observations. For example CO is generally used as a tracer for the total gas in a protoplanetary disk, because it remains in the gas phase over a large radius, and its collisional excitation with H_2 is well understood from observational studies of molecular clouds. While it is assumed that CO should have the same global abundance in disks as it does in molecular clouds ($\sim 10^{-4}$ by number relative to hydrogen), observations of disks have suggested that it does not (Dutrey et al. 1994; Bergin et al. 2013; McClure et al. 2016). Multiple physical (Salyk et al. 2008; Krijt and Ciesla 2016; Xu et al. 2017) and chemical (Bergin et al. 2014; Eistrup et al. 2016; Yu et al. 2016) methods of depleting the CO have been proposed, however this remains an open problem in protoplanetary disk science.

Solids

Left out of the above discussion is the chemical composition of the grains (often called the refractory material) on which grain chemistry occurs. This is because it is generally assumed that the grains condense very early in the disk lifetime. This assumption is supported by the fast (\sim hour) condensation rate timescales that have been observed in lab experiments (Toppani et al. 2006). Because of these fast reaction times (taking place faster than the disk's viscous evolution timescale), equilibrium chemistry methods can be used to compute the chemical abundance of the refractory material.

Equilibrium chemistry utilizes the thermodynamic result that a chemical system in equilibrium will have its total Gibbs free energy minimized. The Gibbs free energy of the system can be expressed as,

$$G_T = \sum_i^N X_i (G_i^0 + RT \log X_i), \quad (5)$$

for a set of N molecules, each with mole fraction X_i , Gibbs energy of formation G_i^0 at a temperature T (Pignatale et al. 2011; Alessi et al. 2017). A second restriction is that the total number of elements:

$$\sum_i^N a_{ij} X_i = b_j \quad (j = 1, 2, \dots, m), \quad (6)$$

where m is the total number of elements in the system and b_j are their initial mole fraction. a_{ij} is the number of the j^{th} element present in the i^{th} molecule (Pignatale et al. 2011; Alessi et al. 2017).

Solving the equations 5 and 6 is generally done with a commercially available software package *HSC*, which has been used in several astrophysical settings (eg. Pasek et al. (2005); Bond et al. (2010); Pignatale et al. (2011); Elser et al. (2012); Moriarty et al. (2014); Alessi et al. (2017)).

Alessi et al. (2017) split the majority of refractories into two primary families: mantle, and core. Core materials are iron and nickel refractories that would settle to the core of a differentiated planet. While mantle materials are silicate, aluminium, and magnesium refractories that would end up in the mantle of a differentiated planet. They report that the primary core materials are iron (Fe), troilite (FeS), fayalite (Fe₂SiO₄), and ferrosilite (FeSiO₃). The primary mantle materials are enstatite (MgSiO₃), forsterite (Mg₂SiO₄), diopside (CaMgSi₂O₆), gehlenite (Ca₂Al₂SiO₇), and hibonite (CaAl₁₂O₁₉).

A third solid that can be tracked with equilibrium models are ices, however thermochemical data in equilibrium software is often incomplete for astrophysically relevant ices like CO₂ and CO. As a result, the only ice that is generally discussed in equilibrium contexts is water.

In Figure 5 (from Alessi et al. (2017)) we show the radial dependence of the core, mantle, and ice material at the disk mid plane, early on in the disk lifetime. The mid-plane solid abundances are quantitatively similar to those found by Bond et al. (2010) and Elser et al. (2012), who also performed equilibrium chemistry calculations on a disc of solar abundance. Over most of the disk there is little variation between the abundance of core and mantle material, apart from the inner (< 1 AU) regions of the disk. In these high temperature regions of the disk, more complex core material like fayalite are less energetically favourable, hence the extra silicon is available to produce more mantle material like enstatite and forsterite (Alessi et al. 2017). As the disk evolves these features move inward with the inward motion of the gas and dust. The abundance of ices show the largest variation, due exclusively to the location of the water ice line (vertical dotted line in Figure 5). This feature likewise moves inward as the disk ages. The large variation in available ice abundance during the formation of planetesimals implies that the resulting composition (and hence structure, see below) will depend on where the initial planet core accretes.

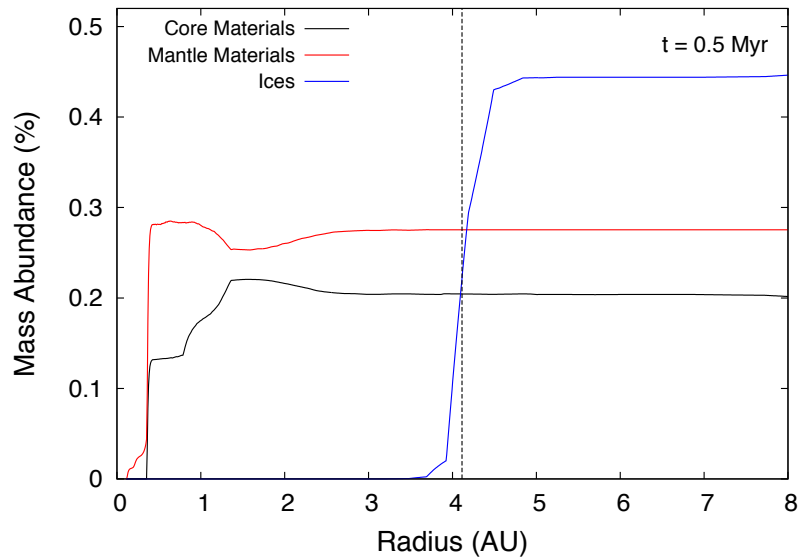


Fig. 5: A snapshot at $t=0.5$ Myr of the radial distribution of cumulative solid materials derived from a thermochemical equilibrium calculation in an evolving disk. Individual silicate and iron based refractories are combined into the more general ‘core’ and ‘mantle’ materials. Where the former will typically end up in the core of a differentiated planet, while the latter would end up in the mantle of a differentiated planet. The two phases of water, solid and gas, are found predominately outward and inward of the water ice line (dotted line) respectively. Figure reproduced from Alessi et al. (2017), MNRAS, 464, 428.

Dust radial drift

As outlined in the chapter by Andrews and Birnstiel, the solid component of the disk (ie. the dust) evolves radially either due to turbulence (when the Stokes number is much smaller than one) or by radial drift (when the Stokes number is near one). This radial drift occurs when a grain is sufficiently large that its dynamics decouples from the gas. When this happens it is no longer affected by gas pressure, and begins to orbit faster than the gas (in Keplerian orbits). This velocity difference produces a head wind on the grain which drains angular momentum, moving the grain to a smaller orbit. The speed at which it drifts is related to the Stokes number (St) through (Weidenschilling 1977):

$$u_{drift} = -\frac{2u_{\eta}}{St + St^{-1}}, \quad (7)$$

where u_{η} is the difference between the dust orbital speed and the gas, and hence the drift is most efficient for grains with $St = 1$.

This drift has important implications for the chemical structure of the disk because dust plays an important role in setting both the opacity of higher radiation (hence impacting the ionization state of the gas), and the rate of gas freeze out (by providing the sites necessary to freeze). Dust radial drift can also act as a transport mechanism for ices because it can transport frozen species across their respective ice lines, enhancing the abundance of gases at these locations.

It has long been known that ice lines could play an important role as the sites for rapid particle growth by condensation. The original suggestion by Stevenson and Lunine (1988) was that there could be a considerable enhancement of material at an ice line from vapour that diffuses from the inner part of the disk. The enhancement of vapour by the evaporation of materials moving inwards across the ice lines was addressed by Cuzzi and Zahnle (2004). Recently, the transport properties of dust grains have been investigated in the context of volatile transport across ice lines (Stammler et al. 2017; Booth et al. 2017; Bosman et al. 2017b). These works have demonstrated that radial drift is sufficiently fast to transport ices across their ice line before sublimation returns the volatile back to the gaseous state. Bosman et al. (2017b) report that grains with a Stokes number of unity (the most susceptible to radial drift) have drift timescales of approximately 100 yr. The rate of sublimation (per volume) is given by (Bosman et al. 2017b):

$$f_{sub} = p_x \sigma_{dust} n_{grain} N_{act} \exp \left[-\frac{E_{bind}}{kT} \right], \quad (8)$$

where p_x is a prefactor, σ_{dust} is the surface area of the dust, n_{grain} is the number density of grains, N_{act} is the number of ice layers available for sublimation (usually 2), E_{bind} is the volatile's binding energy, and T is the temperature of the dust and gas (assumed to be the same). Using the values from Bosman et al. (2017b), and assuming a Stokes number of unity we estimate a reaction time ($n_{H_2O,ice}/f_{sub}$) of a few 100 yr for grains crossing the water ice line. This implies that as the grain crosses the ice line, it does not immediately lose its ice layer. However, because the sublimation rate scales as $\exp(-1/T)$, the grains do not travel far inward of the ice line before losing all of its ice. In fact an increase of only 30 K (radial change of about 0.1 AU for the disk model in Bosman et al. (2017b)) results in a reduction in the sublimation time of 2 orders of magnitude! Once in the gas these enhancements spread out through diffusion, delivering some of the volatile outward of its ice line where it refreezes onto grains - continuing a cycle of freeze out, transport, sublimation, and diffusion (see also Ros and Johansen (2013)). The end result is an enhancement of the C/O within ice lines in the planet forming regions of the disk (Booth et al. 2017), possibly being imprinted into the atmosphere of a forming planet.

Radial drift also plays a role in dictating the ionization state of the gas, because the dust (which contributes highly to the disk opacity) is rapidly cleared from the

outer regions of the disk. Cridland et al. (2017a) showed that when this happens, the region of the disk with low ionization rapidly shrinks, moving the outer edge of the dead zone inward (to ~ 1 AU) quickly (within 1 Myr). Because of its tendency to rapidly drive chemistry, a rapidly changing ionization structure will have an important impact on the chemical structure of the disk. This rapidly shrinking dead zone is at odds with the picture of a laminar accreting disk driven by disk winds (see above). We note however, that the ALMA observations clearly show that radial dust flow in disks is much slower than the current models predict (see the chapter by Andrews and Birnstiel).

A fully self consistent treatment of the dust physics and photochemistry has not yet been undertaken because of technical challenge which include incorporating the radial movement of material in a chemical evolving system of equations. These complexities have begun to be incorporated by Bosman et al. (2017b) for a limited chemical network dedicated to the formation and destruction of CO_2 in disks. However without a full chemical network as seen in Walsh et al. (2014), Helling et al. (2014), Eistrup et al. (2016), or Cridland et al. (2017b) the detailed evolution of the C/O remains elusive.

Planet migration in inhomogenous disks - planet traps

The essence of the standard theory of planet migration in smoothly varying disks was uncovered decades ago. One of the key ideas is that planets can induce the launch of waves at Lindblad resonances in the disk where the forcing frequency of the planet equals the epicyclic frequency of fluids motions oscillating around their guiding Kepler orbits (eg. Goldreich and Tremaine (1979); Ward (1986); Lin and Papaloizou (1986). For torques exerted by the outer and inner Lindblad resonances the corresponding resonances are at epicyclic frequencies of $\kappa(r) = [(m/m + 1); (m/m - 1)]\Omega_p$ respectively, for waves with azimuthal wave numbers m . These exert torques in opposite directions, with the outer resonance (outward angular momentum transport) being the larger as it is closer to the planet due to the gas' sub-Keplerian orbital velocity - a consequence of the local gas pressure gradient. Thus, the net torque generally leads to the planet losing angular momentum.

In these models, if the planet mass is small enough, the disc response is linear. The migration rate is then proportional to the planet and disc masses, independent of the viscosity and weakly dependent on the disc surface density and temperature profiles. This is the so-called Type I migration (Ward 1997). If unopposed, these torques would push an Earth mass orbiting at 1AU into the central star within $\sim 10^5$ years, a timescale that gets shorter as the mass of the planet increases. More detailed analysis of the magnitude of the Lindblad torque that fits the results of 2D numerical simulations to disk models that include the effects of smooth power-law behaviour of the disk surface density $\Sigma \propto r^{-s}$ and the disk temperature $T \propto r^{-\beta}$ were (Paardekooper et al. 2010);

$$\Gamma_L/\gamma\Gamma_o = -2.5 - 1.7\beta + 0.1s \quad (9)$$

where γ is the adiabatic index of the gas and the torque $\Gamma_o = (q/h)^2 \Sigma_p r_p^4 \Omega_p$ can be readily derived by calculating the change in the angular momentum of a fluid element perturbed in passing a planet of mass M_p for quantities evaluated at the position of the planet.

As one comes in closer to the planet and the co-rotation region, parcels of gas undergo nonlinear perturbations and move along "horseshoe" orbits wherein cooler, higher angular momentum fluid to the planet's exterior undergoes a sharp U- turn in front of the planet and swapped into an inner orbit where gas is hotter and has less angular momentum. The opposite occurs for inner fluid moving outwards in the U. Since entropy must be conserved during these motions, a density enhancement near the planet develops resulting in an outward net torque (Ward (1997), Nelson's chapter). Similar effects arise from the conservation of vortensity during these motions. The resulting co-rotation torque was also computed by Paardekooper et al. (2010) and takes the form

$$\Gamma_{HS}/\gamma\Gamma_o = 1.1\left(\frac{3}{2} - s\right) + 7.9(\zeta/\gamma) \quad (10)$$

where $\zeta = \beta - (\gamma - 1)s$ is the power law exponent for the entropy profile of the gas, and the first and second terms address the entropy and vortensity effects. The total torque that a low mass planet undergoes during Type I migration is the sum of these two the Lindblad and horseshoe co-rotation torques; $\Gamma = \Gamma_L + \Gamma_{HS}$.

The values of the power law indices appearing in this combined formula have been worked out for Chambers (2009) disk models (see Cridland et al. (2016)) for an adiabatic index of $\gamma = 1.4$. As has been observed by several authors the net torque is outward in the viscous regime and inward in the radiative regime. This implies that there is a radius of net zero torque $\Gamma = 0$ at the heat transition radius r_{HT} discussed above (Lyra et al. 2010; Hasegawa and Pudritz 2011; Dittkrist et al. 2014). Thus a low mass planet can be trapped at the heat transition, and this cuts off its rapid inward migration. A planetary core trapped there moves with the trap, and accretes materials that are at the trap position as the latter moves through the disk. The evolution of r_{HT} with time is governed by the disk evolution equation discussed above, and in particular depends on the accretion rate, which falls as a function of time as the column density falls, and later as the disk undergoes photo evaporation. These motions are much slower functions of time than the Type I migration time scale because they reflect the slower viscous evolution of the disk which is responsible for the falling accretion rate \dot{M}_a . There is a range of masses that can be trapped in regions of zero net torque. Detailed simulations by Coleman and Nelson (2016) examined the growth of planets that grow in traps caused by radial variations in the disk. These results showed that null points for the torque can trap planets up to 10s of Earth masses. For the more massive planetary cores, being released from the trap will, with rather little additional mass accretion, result in gap opening and the transition to slow Type II migration (see below).

Two other general types of inhomogeneities in disks are possible. Noting that the dead zone must have very low levels of MRI turbulence, while the active regions at larger radii can support active MRI, there is a discontinuity in the dust scale height as one proceeds through the outer dead zone radius. For disk radii $r \leq r_{DZ}$, dust will rapidly settle into the disk mid plane whereas at $r \geq r_{DZ}$, turbulence will keep the dust stirred up to higher scale heights. This means that radiation from the star will see a "wall of dust" at r_{DZ} which will reflect and, as for a garden bed in front of a sunlit wall, will be heated by the back-scattered radiation. This alters the temperature profile of the gas at smaller radii, in such a way as to create a planet trap (Hasegawa and Pudritz 2011; Cridland et al. 2016).

The position of the dead zone, as we have seen, depends on the ionization of the disk and hence is directly connected to ionization driven disk chemistry. A planet trapped at the dead zone radius migrate with the trap's evolution, acquiring a composition reflecting the disk materials encountered as the trap moves inwards through the disk.

The third generic type of disk inhomogeneity is the entire class of ice lines that result from the freezing out of various chemical species on grains. As has already been noted, three of the potentially most important ice lines are those of water, CO, and CO₂. In its most general form, astrochemical models for the disk predict the distribution of ices (eg. water). These results can then be used to compute the change in dust opacity in the disk. This opacity change has a direct effect on the temperature profile across the ice line, which in turn sets the direction of the torque by the temperature dependence of equation 9. In order to have a sufficient large change in the opacity across an ice line, one can anticipate that the relevant volatile must be abundant - as is the case for water (Miyake and Nakagawa 1993). Water ice lines have accordingly been suggested as trapping points for planets (Ida and Lin 2008b; Hasegawa and Pudritz 2011).

Why does an ice line act as a potential trap? At the ice line, the opacity κ is reduced as the dust grains are coated with ice, and the associated cooling rate of the gas is increased (since the cooling rate $\propto 1/\kappa$; (Bitsch et al. 2013)). Coupled to the cooling rates, the local temperature and thus the disk scale height, is reduced ($H = c_s \Omega \propto T^{1/2}$). Since the disk accretion rate is constant across the disk at any instant, and because the viscosity is dependent on the local gas temperature ($\nu \propto c_s H \propto T$), a reduced temperature results in an enhancement in the local surface density at the ice line to maintain a constant mass accretion. Both the modified temperature and density gradients impact the net torque, resulting in a trap.

Detailed analysis of opacity effects at ice lines indicate that water is sufficiently abundant (1.5×10^{-4} molecules per H) to trap planets at its ice line due to an opacity transition. Volatiles that have mass abundances lower than a factor of ~ 40 with respect to water do not result in a sufficiently strong opacity transition to trap planets in a disk that is viscously heated as shown in numerical simulations (Cridland, Pudritz, & Alessi, in press). These results suggest that CO, while sufficiently abundant, also does not trap planets at its ice line. This is because its ice line is in the outer parts of the disk where heating is dominated by irradiation by the host star rather than viscosity. In this heating regime, the midplane temperature is not as dependent

on the dust opacity, and hence an opacity transition does not cause a strong change in the temperature profile as seen at the water ice line. Like water, the CO₂ ice line occurs in the viscously heated part of the disk and hence could act as a trap. However it is not easily produced in the gas phase, and hence its availability as a trap depends on your choice of initial conditions (dark cloud vs. diffuse ISM chemistry) and chemical network (gas only vs. gas-grain chemistry).

We reach an interesting and important conclusion about planetary migration that has direct consequences for both planet formation and composition. Low mass planetary embryos move along with traps that move inwards through the disk as it evolves on a viscous time scale. Planets eventually break away from their traps when they become sufficiently massive as shown in numerical simulations of (Coleman and Nelson 2014) - typically up to 10 Earth masses. The solid materials accreted during this time reflect the composition of the evolving disk visited by the relevant trap. The heat transition, being typically the furthest out in the disk, is beyond the ice line and so planetary cores can be expected to have a strong contributions of ices (Alessi et al. 2017). A core building at the ice line would be expected to have less ice, and a dead zone, which is often inside the ice lines, would be expected to have a very small ice content. Detailed simulations bear out these general results (see subsection on solids).

The dynamics of embryos as they approach planet traps has not yet been investigated in any detail. One anticipates that a rapidly building core may scatter incoming materials. As a planet builds in a trap, one also anticipates that a chain of embryos will come into mean motion resonances with the traps, resulting in a series of planets undergoing accretion associated with each trap.

As the mass of planets increase, the angular momentum exchange between disk and planet can lead to the opening of a gap, a process called Type II migration (Ward 1997). In this regime, a balance is established between the tidal torque which tends to open a gap (inner material has angular momentum removed and moves inward, which is then transferred via the planet to the outer material which moves outwards) - and viscous torques which always act to fill in a gap.

The ‘gap opening’ mass requires the planet’s Hill radius to be larger than the pressure scale height at the planet’s location, otherwise the gap will be closed by gas pressure. A second requirement is that the torques from the planet on the disk exceeds the torques caused by viscous stress. These requirements are summarized by, (Lin and Papaloizou 1993; Hasegawa and Pudritz 2011),

$$\frac{M_p}{M_*} = \min[3h_p^3, \sqrt{40\alpha_{turb}h_p^5}] \quad (11)$$

where $h_p = H/r_p$. The depth and width of the gap depend on this balance (Papaloizou and Lin 1984). The Lindblad resonances which drive the disk-planet angular momentum exchange fall into opening gap and therefore the migration rates are drastically reduced compared to Type I. The planet then becomes locked to disk migration at the radial velocity of $u_r = v/r$, and the disk is essentially split into an inner and outer region. This result is based on the assumption that gas doesn’t enter the gap once formed. This, is in fact to simplistic a view since horseshoe orbits can

readily facilitate a flow through the gap. Numerical studies carried out by Crida and Morbidelli (2007) and Edgar (2008), have recently been generalized by Duffell et al. (2014) who showed that Type II migration can, on this basis, be faster or slower than the viscous rate depending on disk parameters such as the turbulent Mach number.

One of the main results of the early population synthesis studies arose when the effects of Type I planetary migration (Ida and Lin 2008a) were considered. Synthesis studies of planets migrating in evolving, standard, Shakura-Sunyaev smooth disks showed that rapid loss of such bodies occurs within 10^5 yrs. The model introduced a parameter - a slowing down factor - needed in order to match predicted and observed populations in the M-a diagram. The result was that standard migration in smooth disks needed to be slowed down by a factor of 30-300 (see Nelson's review) - i.e. - slowed to speeds more reflecting viscous evolution of the disk. The theory of planet traps, sketched above, provides a physical solution for this problem.

The results of planet migration on planetary populations and their evolutionary tracks in the M-a diagram are discussed in the following section. We emphasize that these are a consequence of a treatment of co-rotation torques that depend on disk viscosity. In MHD wind driven regions (eg. the dead zone) disks may be considered to be inviscid and there, co-rotation torques will arise from MHD disk winds (McNally et al. (2017), review in Nelson's chapter). Here, the shape of the horseshoe orbit region near the planet can be modified by the winds, leading to a more "history-dependent" evolution of the horseshoe torque.

Planet formation & composition

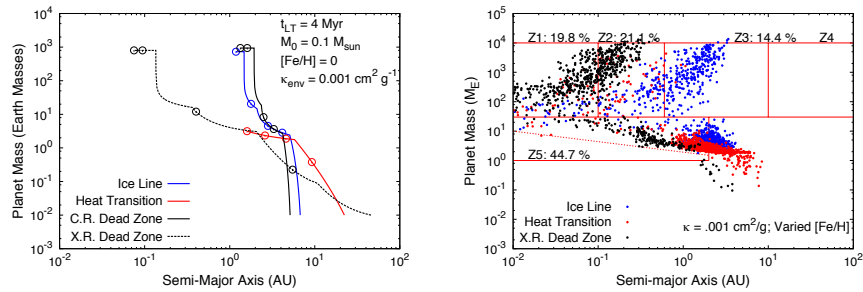
The process of planet formation is complex and involves growth from interstellar dust ($\sim \mu\text{m}$) up to Jupiter-sized planets ($\sim 10^5$ km), a range of 14 order of magnitude! Of course modelling the complete process is impossible, and hence most models begin or end at an intermediate stage called a planetesimal (size between 1-100 km).

Growth from interstellar dust to planetesimals requires crossing the 'meter-barrier' - a size where fragmentation and radial drift destroys the object faster than it can grow (see chapter by Andrews and Birnstiel) . A method for circumventing the meter-barrier is through the streaming instability (Youdin and Shu 2002; Youdin and Goodman 2005; Raettig et al. 2015; Schäfer et al. 2017). Simulations by Simon et al. (2016) found that the resulting planetesimal mass distribution scales as $dN/dM_p \propto M_p^{-1/6 \pm 0.1}$ up to objects on the scale of the large asteroids or Kuiper Belt objects. Hydrodynamic simulations of the streaming instability can rapidly build up a population of planetesimals available for further growth (Johansen et al. 2007; Schäfer et al. 2017).

There are two primary methods of solid accretion to grow planets from the initial planetary embryo: planetesimal accretion and pebble accretion. The primary difference between planetesimal and pebble accretion is the size of the accreting mass. Pebble accretion assumes that the planetary embryo is accreting $\sim\text{cm}$ sized

‘pebbles’ rather than km-sized planetesimals. As a result the effective gravitational focusing is much higher for pebbles because their speed relative to the embryo is much smaller than planetesimals (Bitsch et al. 2015).

Both of these mechanisms grow a planetary core with a mass of between 5-10 M_{\oplus} , at which point the planetary core begins to accrete its gaseous atmosphere (see the chapter by Mordasini for details). Gas accretion occurs in two phases - a slow phase where the planetary envelope remains connected to the surrounding protoplanetary disk gas, and a fast phase where the planetary envelope decouples from the disk. These two phases, along with the initial phase of solid accretion can be seen in Figure 6a.



(a) Individual planet formation tracks representative of 3 different planet traps.

(b) Full synthesized population of planets. The colour code is for planets formed on the three different planet traps

Fig. 6: Sampling many planet formation tracks (see a) with different disk initial conditions and physical parameters is used to construct a synthetic population of planets (see b). Comparing the occurrence rate of different types of planets to the observed population helps to constrain the physical properties of the protoplanetary disk and the growing planet which lead to the observed population of planets. Figures reproduced from Alessi and Pudritz (2018), arXiv:1804.01148 (submitted to MNRAS).

In Figure 6a we show individual formation tracks (the evolution of a planet through the mass-semi-major axis diagram) for a typical growing planet in three traps indicated by the colour code. The size and evolution of dead zones in disks depends on the type of disk ionization that dominates. In this model, a constant dust to gas ratio is assumed for the gas. Shown in the figure are tracks for planets in dead zone traps, for disks ionized either by cosmic rays (C-R deadzone) or X-rays (X-R deadzone). Planets generally evolve from right to left, and bottom to top of the diagram following the traps as they move slowly inward through the disk on 10^6 year type of time scales. Planet evolution tracks start in planet traps as the embryos are assumed to migrate very quickly until they encounter a trap. They then begin

their growth in the Oligarchic stage (see Kokubo and Ida (2002) and Ida and Lin (2004a)) by accreting solids until the majority of solids have been cleared out of the planet’s feeding zone. The timescale associated with this accretion ($\sim 10^5$ yr) is much shorter than the migration timescale ($\sim 10^6$ yr) if the planet begins close (< 10 AU) to the host star. So the planet evolves nearly vertically on the diagram (see the blue and black curves). Farther out in the disk, the solid accretion rate is comparable to the migration rate, and the planets evolve more diagonally (red and black dashed line). Once the rate of solid accretion drops, the core can cool to begin accreting gas, and enters into a phase of slow gas accretion.

Beginning in this slow phase of accretion, the gas is first accreted into an envelope that remains connected with the surrounding disk, but slowly contracts. This contraction is limited by the rate that the envelope can radiate its energy away, and hence contracts on the Kelvin-Helmholtz timescale (Ida and Lin (2004a), or see the chapter by Mordasini). In this phase the contraction occurs at a slower timescale than the (trapped) migration timescale ($\sim 10^6$ yr), and the planet evolves nearly horizontally across the diagram.

For masses exceeding a critical mass $M_p > M_{c,\text{crit}}$, gravitational instability ensues and the planet’s gas envelope grows by accretion from the disk on the Kelvin-Helmholtz timescale (Ikoma et al. 2000),

$$\tau_{KH} \simeq 10^c \text{ yr} \left(\frac{M_p}{M_\oplus} \right)^{-d}. \quad (12)$$

The values of parameters c and d in the Kelvin-Helmholtz timescale are physically linked to the opacity of the accreting planet’s atmosphere, κ_{env} . This is included in the model by using the fits shown in Mordasini et al. (2014), that relate results of a numerical model of gas accretion to the Kelvin-Helmholtz parameters for a range of envelope opacities of $10^{-3} - 10^{-1} \text{ cm}^2 \text{ g}^{-1}$. The fit given for the Kelvin-Helmholtz c parameter is, $c = 10.7 + \log_{10} \left(\frac{\kappa_{\text{env}}}{1 \text{ cm}^2 \text{ g}^{-1}} \right)$. The Kelvin-Helmholtz d parameter has a more complicated dependence on envelope opacity, ranging from $\approx 1.8-2.4$ over the range of κ_{env} considered, the details being given by a piecewise-linear function shown in Mordasini et al. (2014).

Once the planet becomes sufficiently massive the contraction becomes rapid and the envelope decouples from the surrounding disk. In this rapid phase the gas accretion timescale ($\leq 10^4$ yr) is much lower than the migration timescale, and hence the planet again evolves nearly vertically. Clearly this unstable phase must not last long, and there have been multiple suggests to limit the rate of gas accretion. One way is to simply place an upper limit on the mass of the planet. This limit is often set as a large ($\sim 50 - 100$) multiple of the gas opening mass (see Hasegawa and Pudritz (2013) and Alessi et al. (2017)). Alternatively, the gas accretion can be limited by other accretion rates once a gap is opened in the disk. In these models, the gas accretion is limited by the Bondi accretion rate, or the global disk mass accretion rate (see above). Because the majority of the gas mass is accreted during this fast accretion phase, changing the gas accretion prescription could result in changes in

the chemical composition of the gas as it accretes onto the planet. Whether these would be measurable changes has not yet been investigated.

In Figure 6b we show results from a population synthesis of our formation model (Alessi and Pudritz 2018). Each planet has evolved through different regions of the disk at different times, because they are the result of different disk initial conditions and parameters, and hence have accreted gas with potentially different chemical histories. A key result from this population synthesis study is that a reasonable fit to the observed M-a diagram with its separated hot and warm Jupiter populations, such as shown in this figure, required a low envelope opacity ($\kappa_{env} \simeq 0.001 \text{ cm}^2 \text{ g}^{-1}$) that is three orders of magnitude smaller than the opacity of materials in the disk. Higher envelope opacities lead to inefficient cooling and lower accretion rates, which means that the planets are dragged into the inner regions of the disk before they start accreting much mass. This, in effect, washes out the warm Jupiter population.

Another result seen in this population study is that the warm Jupiters are primarily formed in the ice line trap - a conclusion also reached by Hasegawa and Pudritz (2013) and first suggested in Ida and Lin (2008a). Of particular interest is that low mass super Earths do not appear in the innermost regions (less than 0.1 AU) of the M-a diagram. This may be a consequence of the model in that dust does not undergo radial drift. If it did, it may be possible to populate this region, but this remains to be computed. Hasegawa (2016) has indeed noted that another formation mechanism - such as terrestrial planet formation - may be needed to explain the low mass planets that end up in such close in orbits.

With the kind of machinery that has been discussed here, one is in a position to compute the chemical composition of the material that is accreted during the planet formation process. These models are called either ‘end-to-end’ or ‘chain’ models because they link physical and chemical models together in succession. A generally construction of these end-to-end models is *disk model* \rightarrow *chemical model* \rightarrow *planet formation & migration*. Variations and extensions of this general chain have been made, including a dust evolution model (Cridland et al. 2017a) and a planetary atmosphere model which includes the generation of synthetic spectra (Mordasini et al. 2016). The chemical model can be construct empirically (Mordasini et al. 2016), through chemical equilibrium models (Alessi et al. 2017), or from time-dependent chemical models (Cridland et al. 2017b), depending on the focus of the chain.

Planet Cores

The physics of planetary interiors and cores depends on the equations of state (EOS) of the primary materials such H, He, and materials made of water, silicates, and iron - as well as the overall chemical composition of the planet (see review Baraffe et al. (2014)). Knowledge of the first aspect of this problem relies on experimental studies of the properties of materials under high pressure, as well as by satellite probes of the density structures of the giant planets such as Jupiter, recently achieved

by the Juno mission (Bolton et al. 2017). It is in the second aspect - the range in overall compositions of planets that give rise to the enormous diversity to the M-R relations for planets. The elemental composition of planets is directly connected to the materials planets accreted as they were formed. Thus, the structural properties of planets as seen in their M-R relation, are a direct consequence of planet formation.

The observations show that exoplanets are incredibly diverse. In Figure 7, left panel (Howard et al. 2013), we observe that planets with a given mass can have an enormous range of sizes. Thus for the Jovian planets, (a few hundred Earth masses), one observes of a factor of 2 range in planetary radius for a given mass. One also notes that there are "inflated" Jovian planets whose radii greatly exceed those predicted for a composition of pure hydrogen. A variety of models have been proposed to explain such planets including stellar heating (Showman and Guillot 2002; Weiss et al. 2013) and heavy element gradients in the planetary interior that would decrease the rate of heat transport thereby slowing down the cooling and contraction of the planet (Chabrier and Baraffe 2007). Similarly, for Super Earth masses, there is a wide range of radii for any given mass again indicative of planets that are composed of a very wide range of materials. The right panel of Figure 7 is a blow up of the Super Earth mass regime (1 - 10 Earth masses), and clearly shows the existence of planets with densities corresponding to rock-iron mixtures.

The effects of heavy metal enrichment on planet structure were first carried out by (Zapolsky and Salpeter 1969), for planets made of individual elements at $T = 0$. If convective energy transport dominates in the planetary interior, the temperature gradient will be nearly adiabatic. As is seen from Figure 7a, increasing the heavy element content in giant planets leads to a decrease in their radii. Composition gradients within their interiors suppress their interior cooling, leading to models that are hotter than the adiabatic models (Leconte and Chabrier 2013).

The core accretion picture of Jovian planet formation predicts the existence of rocky, 10 Earth mass cores (Mizuno et al. (1978); Bodenheimer and Pollack (1986); Pollack et al. (1996) - and chapter by D'Angelo and Lissauer) What evidence is there for this picture? And what chemical state is the interior of the planet in? If Jovian planets form by gravitational instability, then there would be no initial core. If a core did form, it could erode away with time as it slowly dissolves in liquid metallic hydrogen (Stevenson 1985; González-Cataldo et al. 2014) enriching the envelope above it.

These fundamental questions were addressed by one of the most significant experiments in planetary science over the last decade - the Juno spacecraft. The mission goal is to improve our understanding of the origin and evolution of Jupiter, the history of the solar system, and planetary system formation in general. On August 27, 2016, this probe flew less than 5000 km over the equatorial cloud tops of Jupiter acquiring a wealth of measurements of the state of the planet's atmosphere, magnetic field, and interior structure (Bolton et al. 2017). The gravity measurements, found by determining small deviations of the spacecraft trajectory due to low order harmonics (J_4, J_6 in particular) of Jupiter's gravitational field, were an order of magnitude more sensitive than any before it.

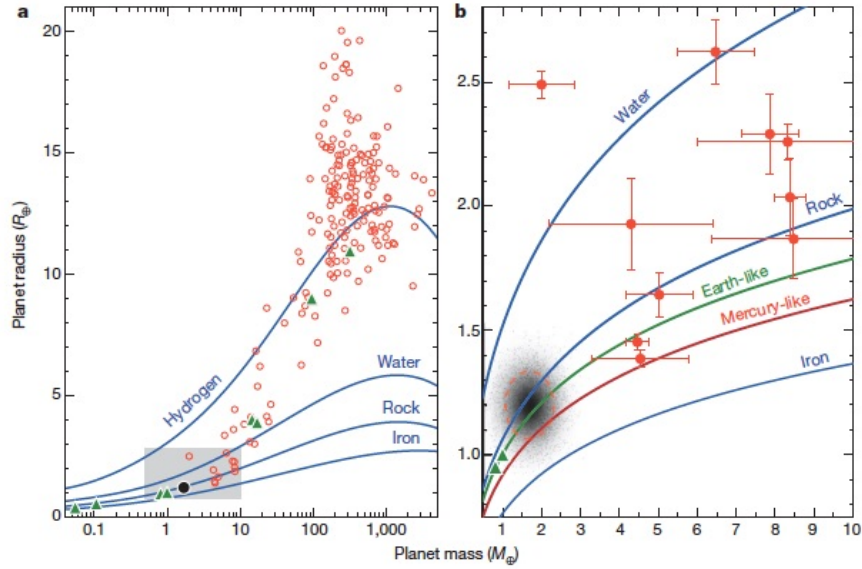


Fig. 7: The planet mass-radius (M-R) diagram for a set of Hot Jupiters and sub-Earths. In the left panel, the M-R curves denote planets that are made from pure hydrogen, water, rock and iron. The right panel is a blow up of the greyed region in the left panel, and additionally shows the M-R curves for Earth-like, and Mercury-like planets. Clearly there is a diverse set of compositions in the super-Earths (right panel) as no internal model uniquely describes every planet. Likewise, Hot Jupiters (left panel, top right) can be highly irradiated, and hence are ‘puffier’ than the hypothetical ‘pure hydrogen’ planet. Figure from Howard et al. (2013), *Nature*, 503, 381. Reproduced with permission ©Springer Nature.

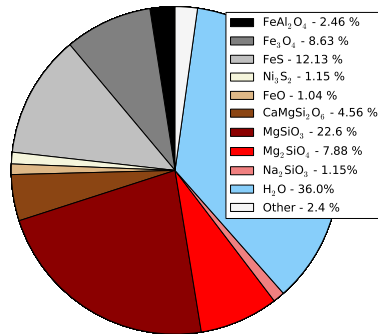
The modelling of the planetary interior and comparison with the data (Wahl et al. 2017) considered interior density profiles that are in hydrostatic equilibrium;

$$\nabla P = \rho \nabla \Phi \quad (13)$$

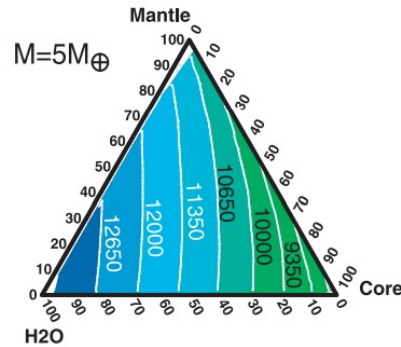
where a barotropic pressure $P(\rho)$ corresponding to isentropic profiles constructed from various EOS is used. Numerical simulations of H-He mixtures from (Militzer and Hubbard (2013), MH13) were employed. Density functional theory molecular dynamics simulations are the best technique for determining densities of hydrogen-helium mixtures over most of conditions in a giant planet ($P > 5$ GPA).

The results show that Jupiter has a core in the range of 6-25 Earth masses. The results are generally consistent with the core accretion - collapse model (Pollack et al. 1996). The larger masses correspond to having a more dilute density profile in the core, equivalent to extending about 10 Earth masses of material out to 0.3-0.5 Jovian radii, R_J . This agrees with models that account for the dissolution of

planetesimals (Lozovsky et al. 2017) as the reason for a dilute core structure. It is not known whether there is enough convective energy available to lift so much material. The overall results clearly depend on exactly how the planet formed, and how mixing occurred during these early stages (Leconte and Chabrier 2012). The mass of the heavy elements in the envelope depends strongly on the EOS, with MH13 predicting 5-6 times solar heavy metal fraction in Jupiter.



(a) A breakdown of the refractories that are accreted into a Super Earth with a final mass of 5.4 Earth masses, formed at the heat transition trap r_{HT} , in a calculation with a disk life time of 3 Myr. Figure reproduced from Alessi et al. (2017), MNRAS, 464, 428.



(b) Ternary diagrams showing results of planet interior structure calculations. The radius (shown in units of km) of a super Earth is dependent on the planet's total mass, as well as the mass distribution among water, core (irons and nickels), and mantle (Mg/Al/Ca silicates) components. Figure from Valencia et al. (2007), ApJ, 665, 1413. Reproduced with permission ©AAS.

Fig. 8: The link between a super-Earth's size and its internal composition is complicated, but generally dominated by the abundance of ice that it accretes and retains during its formation.

Planets will acquire their rocky materials while migrating through the disk in planet traps, accreting materials characteristic of those traps (eg. ice lines). The movement of the trap through the evolving disk determines the cumulative inventory of all of the different kinds of solid materials that are accreted along the way (Alessi et al. 2017). Figure 8.a shows the detailed breakdown of materials accreted from the disk by a forming super Earth planet moving with the heat transition trap. The final mass in this model reaches 5.4 Earth masses. In this calculation, the ice fraction is 36 %, the mantle 36 %, and core materials 27 %. Since cores trapped at the heat transition will spend most of their life beyond the water ice line, these will generally have the greatest ice mass fractions. Planets trapped at the water ice line will have a smaller proportion of ice, while dead zone planets will have the least since the dead zone radius occurs typically inside the ice line. As an example of the sensitivity of

the compositions of Super Earth compositions to disk parameters, planets formed in a disk with a 2 Myr life time in the heat transition planet had an ice content reached 48 %, whereas for the dead zone planets only reached 6 %.

As was the case for solids, gas abundances of planet atmospheres will reflect the temperature of the regions in the disk where they accreted material. Abundances of CO, N₂ and SiO result from gas accretion in hot regions of the disc, while accretion from colder regions of the disc results in higher abundances of H₂, O, CH₄, and NH₃. These results clearly illustrate how a wide range of bulk densities of planets can arise when one considers variations across disk populations (eg. different lifetimes), as well as the type of traps planets accrete their materials from. This gives some explanation for the wide scatter seen in the M-R diagram.

The materials delivered to a planet during the accretion phase are of course modified as a consequence of the P-T relations in the planet interior and atmosphere. Terrestrial planets are modelled as having a crust, mantle, liquid core, and a solid core. The most massive of these are the mantle and the core, comprised of silicates and iron alloys. These differentiated from one another because iron is denser than silicates. Four elements (oxygen, iron, magnesium and silicon) account for 95 % of the total mass of the Earth (Javoy 1995).

The M-R relation for rocky material at constant density is $R \propto M^{1/3}$. The dependence of the M-R relation on the types of materials in the planet can be simplified by considering just 3 basic types of materials; ice, mantle materials, and iron (the latter two being categories containing many minerals). Following the early work on zero temperature models for single compositions by Zapolsky and Salpeter (1969), Valencia et al. (2007) built models that include all three of these basic materials. Here, the P-T relation diagram is computed using EOS used for modelling the Earth. The results of such calculations are illustrated in terms of ternary diagrams often used in Earth sciences (Figure 8b). Data for this three component system are plotted along the sides of a triangle, representing each of these basic materials. Each vertex means 100 % of a particular component, and data plotted on the opposite side mean 0 %. Lines parallel to a particular side will show various degrees of a component whose maximum value is shown at the corresponding opposite vertex. The M-R relationship is found to take a power law form $R \propto M^\beta$ where $\beta = 0.262(1.0 - 0.3IMF)$ and IMF is the percentage amount of water. For super Earths, pressures will be much higher and so different EOS are required. This M-R power law exponent is actually less than 1/3 (0.274) because as the density increases with increasing pressure while the temperature remains roughly constant (Grasset et al. 2009).

Atmospheres

A key observable in studying the chemical composition of exoplanetary atmospheres is the carbon-to-oxygen ratio (C/O). This is because (as we have said before) it can be naturally linked to chemical processes in the protoplanetary disk, and also

because the elemental ratio is less sensitive to chemical processes within the atmosphere.

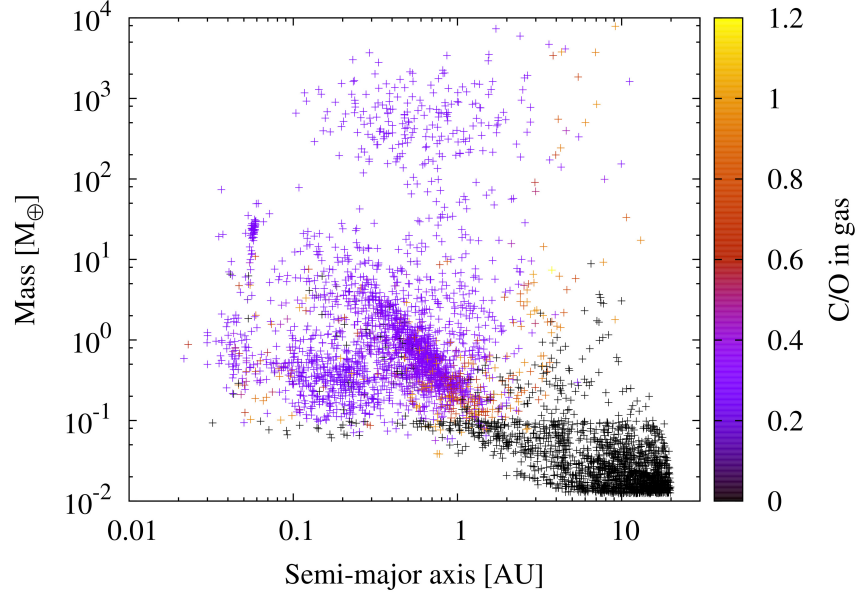


Fig. 9: Distribution of C/O in the atmosphere of planets across a population synthesis model. In this model the molecular abundances are held constant, and hence the C/O of the planetary atmosphere is generally dominated by the accretion of gas. Figure from Thiabaud et al. (2015), A&A 574, A138. Reproduced with permission ©ESO.

In Figure 9 we show a population synthesis model that included enough simple chemistry to estimate the resulting C/O (from Thiabaud et al. (2015)). In their work, Thiabaud et al. (2015) showed that the resulting C/O in a planetary atmosphere is dependent on the chemical evolution of the disk, the migration and accretion history of the planet, and the modelled physical structure of the protoplanetary disk. In the figure, the radial distribution of the disk's molecular abundances is held constant throughout planet formation, similar to the assumptions made to construct 4 by Öberg et al. (2011b). However, Thiabaud et al. (2015) also include a model where the gas diffuses inward as the host star accretes material through the disk. In this model, the planetary C/O is dominated by the accretion of ices, this is discussed below.

Thiabaud et al. (2015) initialize their disk model with C/O that is approximately solar (0.54). Generally it is assumed that the disk's initial C/O (in both gases and solids) matches the stellar C/O that can be observed today. They find that most planets have sub-stellar C/O (< 0.3), while some of their planets resulted in super-

stellar C/O . This result depended on their choice of chemical model, and in the case that ice accretion dominated the C/O , nearly all planets had sub-stellar C/O . The majority of their high mass, close-in planets (ie. Hot Jupiters) generally have sub-stellar C/O which disagrees with the observations of Brewer et al. (2017).

A similar conclusion was reached by Mordasini et al. (2016), and as in the case of the majority of models run by Thiabaud et al. (2015), C/O is dominated by the accretion of ices. In Cridland et al. (2017b) C/O is dominated by the accretion of the gas, and because of their migration model, most of the planets accrete their gas near the water ice line, resulting in planetary C/O which matched the initial gas C/O of the disk. A key difference between models which are dominated by gas and ice accretion is in their treatment of the chemical abundance of the gas.

In the evolving models of Thiabaud et al. (2015) and in Mordasini et al. (2016) the gas is assumed to be ‘pristine’ - only consisting of H/He - while the higher metallicity gas is accreted onto the host star. However, Cridland et al. (2017b) compute the chemical evolution of the gas while ignoring the radial accretion of the gas through the disk. Observations of protoplanetary disk (Henning and Semenov 2013), along with simulations which include chemistry, gas evolution, and dust radial drift (Bosman et al. 2017a), tend to disfavour pristine gas in the planet forming region of the disk.

In Figure 10a we show a set of planet tracks used in Cridland et al. (2017b). Each track denotes the evolution of a planet in each individual planet trap, and we label the time (in Myr) when the planet appears at a given position. Along side these tracks we note the location of the water ice line with vertical dotted lines at 1-4 Myr.

In Figure 10b we show the molecular abundance of the atmospheres accreted by the planets from the left panel. While the C/O and the C/N (carbon-to-nitrogen ratio) are the same in each of these planetary atmospheres, their initial molecular abundance can differ. In particular Cridland et al. (2017b) report a difference in the abundance of the primary nitrogen carriers (N_2 and NH_3). The planet which accreted its gas early (the ice line trapped planet) primarily accreted NH_3 while the two planets that accreted later in the disk evolution accreted primarily N_2 . This highlights an important additional restriction on chemical composition of planetary atmosphere. Because of chemical evolution in the protoplanetary disk, *when* and *where* a planets accretes its gas will impact the molecular abundance that is inherited by the planet’s atmosphere.

Further complicating this problem are the effects that enrichment from solids can have on a planet’s atmospheric composition. There are two important effects to consider that can lead to atmospheric enrichment from solids: (i) Solids accreted from the disk onto a planet with an atmosphere can be disrupted or ablated (Pinhas et al. 2016) instead of accreting directly onto the core. This effect has also been recently considered to investigate the maximum masses of cores that can be built up by accretion of pebbles (Alibert 2017; Brouwers et al. 2017). (ii) As was discussed in Madhusudhan et al. (2017), a planetary core can be eroded by the massive atmosphere of a gas giant. Convective motions throughout a Jovian atmosphere can mix the eroded, metal-rich material throughout the atmosphere, changing its composition and C/O ratio. These effects suggest that that accretion rates and compositions

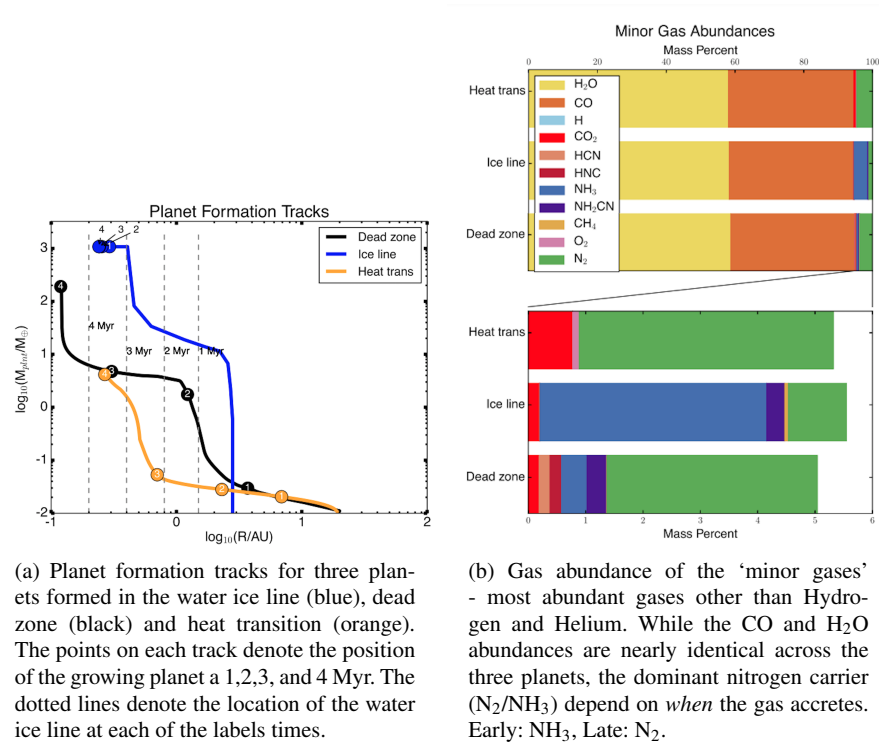


Fig. 10: Molecular abundance results for planet formation in an astrochemically evolving disk model. Here we see that *when* a planet accretes its gas can be as important as *where* it accretes because the molecular gas can undergo chemical evolution on a similar timescale as the planet formation process. Figures reproduced from Cridland et al. (2017), MNRAS, 469, 3910.

of both gases and solids need to be considered to fully understand the compositions of planet atmospheres throughout the formation phase.

An important result overall is that intermediate size, low-velocity planetesimals of 90 - 250 metres can penetrate through a massive envelope and reach the core. These objects are too small to attain the velocities required for frictional ablation and yet too large to be heated to the melting temperature. The key question then becomes - at what point in the growth of the atmosphere and migration of the planet were conditions most favourable for planetesimal accretion to the core, and what fraction of the overall solid accretion was this? The answer to this question clearly involves a much better understanding of coupled migration and accretion.

Once in the atmosphere the gas can evolve both physically and chemically between when it was accreted and when it is observed. These processes are complex, and their study involve three-dimensional hydrodynamic simulations (eg. Cooper

and Showman (2006)), time-dependent photo-chemical networks (eg. Agúndez et al. (2014)), and synthetic spectra (eg. Mollière et al. (2017)). As it stands, no complete model of exoplanetary atmospheres has been developed, and the observations of chemical complexity in atmosphere remain in their early stages of development. With the next generation of space and ground based telescopes we will soon see exoplanetary atmospheres in a new light.

Conclusions

Having reviewed the basic processes involved in an end-to-end picture of planet formation, we return to our original question. Are there clearly discernible links between the chemical and physical structure of planets, and their formation history? We have seen that on the observational side, JWST is likely to revolutionize our understanding of the composition of planetary atmospheres. On the theoretical side, new ideas related to angular momentum transport by MHD disk winds as well as the role of pebble accretion are still very much in development. And finally, the Juno results which have shed so much new light to the problem of Jupiter's structure and origin are still being derived. We are likely to be on the cusp of a radically new picture of planet formation and composition as these results solidify over the coming 5 years. Be that as it may, one can still discern some important emerging patterns.

- **The core accretion picture has ever more empirical support.** The results of the Juno probe and the ability of such models to understand the mass-metallicity relation and many aspects of observed planetary populations appear to give this picture a growing amount of empirical and theoretical support.
- **Migration and traps have a direct effect on the kinds of materials that planets accrete.** The fact that planets accrete most of their solids while in particular kinds of traps gives them special kinds of "diets" that are preserved in the element ratios of their cores and atmospheres. More work is needed to perfect our ideas of traps and migration, but because these are connected to both disk chemistry and angular momentum transport, element patterns arising from accretion probably persist.
- **Dust evolution is critical.** The movement of dust in protoplanetary disks affects all aspects of disk ionization, disk chemistry, and ultimately on the nature of the solids that are accreted by growing, migrating planets. We do not yet have a final picture of dust evolution in disks, but observations from ALMA and JWST may help considerably in building more comprehensive physical theories of dust evolution in disks.
- **Accretion vs dissolution in massive planet interiors.** The Juno results underline some of the important and lingering uncertainties in theoretical modelling of the formation of massive planets. Jupiter's core could be slowly dissolving since its formation, or, planetesimals may not have reached the core and dissolved instead in the envelope. The pattern of chemical enrichment will be different in

these two scenarios so greater effort needs to be applied to understanding the detailed fates of planetesimals as they accrete into the atmospheres of giant planets during formation.

While no clear cut answer to the question is possible at this point, there are reasons to expect that these links do indeed exist. Elucidating them will require the best new instruments, observatories, and calculations that we can muster over the next decade.

Acknowledgements

We thank Phil Armitage for his very useful referee report. We also thank Yasuhiro Hasegawa, Ted Bergin, Til Birnstiel, Christoph Mordasini, Thomas Henning, Dmitry Semenov, Nikku Madhusudhan, Richard Nelson, and Colin McNally for enlightening discussions during the course of this project. This research was supported by a Discovery grant to REP from the Natural Sciences and Engineering Research Council of Canada (NSERC), as well as by NSERC postgraduate scholarships to AC and MA.

References

- Agúndez M, Parmentier V, Venot O, Hersant F, Selsis F (2014) Pseudo 2D chemical model of hot-Jupiter atmospheres: application to HD 209458b and HD 189733b. *A&A*564:A73
- Alessi M, Pudritz RE (2018) Formation of Planetary Populations I: Metallicity & Envelope Opacity Effects. *ArXiv e-prints*
- Alessi M, Pudritz RE, Cridland AJ (2017) On the formation and chemical composition of super Earths. *MNRAS*464:428–452
- Alibert Y (2017) Maximum mass of planetary embryos that formed in core-accretion models. *A&A*606:A69
- Alibert Y, Mordasini C, Benz W (2011) Extrasolar planet population synthesis. III. Formation of planets around stars of different masses. *A&A*526:A63
- ALMA Partnership, Brogan CL, Pérez LM et al. (2015) The 2014 ALMA Long Baseline Campaign: First Results from High Angular Resolution Observations toward the HL Tau Region. *ApJ*808:L3
- Andrews SM, Williams JP (2007) High-Resolution Submillimeter Constraints on Circumstellar Disk Structure. *ApJ*659:705–728
- Andrews SM, Wilner DJ, Hughes AM, Qi C, Dullemond CP (2010) Protoplanetary Disk Structures in Ophiuchus. II. Extension to Fainter Sources. *ApJ*723:1241–1254
- Armitage PJ (2010) *Astrophysics of Planet Formation*
- Bai XN (2014) Hall-effect-Controlled Gas Dynamics in Protoplanetary Disks. I. Wind Solutions at the Inner Disk. *ApJ*791:137
- Bai XN (2016) Towards a Global Evolutionary Model of Protoplanetary Disks. *ApJ*821:80
- Bai XN, Stone JM (2013) Wind-driven Accretion in Protoplanetary Disks. I. Suppression of the Magnetorotational Instability and Launching of the Magnetocentrifugal Wind. *ApJ*769:76
- Bai XN, Stone JM (2017) Hall Effect-Mediated Magnetic Flux Transport in Protoplanetary Disks. *ApJ*836:46

- Balbus SA Hawley JF (1991) A powerful local shear instability in weakly magnetized disks. I - Linear analysis. II - Nonlinear evolution. *ApJ*376:214–233
- Banerjee R Pudritz RE (2006) Outflows and Jets from Collapsing Magnetized Cloud Cores. *ApJ*641:949–960
- Baraffe I, Chabrier G, Fortney J Sotin C (2014) Planetary Internal Structures. *Protostars and Planets VI* pp 763–786
- Batalha NM (2014) Exploring exoplanet populations with NASA's Kepler Mission. *Proceedings of the National Academy of Science* 111:12,647–12,654
- Bate MR (2012) Stellar, brown dwarf and multiple star properties from a radiation hydrodynamical simulation of star cluster formation. *MNRAS*419:3115–3146
- Bate MR (2018) On the diversity and statistical properties of protostellar discs. *MNRAS*475:5618–5658
- Benz W, Ida S, Alibert Y, Lin D Mordasini C (2014) Planet Population Synthesis. *Protostars and Planets VI* pp 691–713
- Bergin EA, Cleeves LI, Gorti U et al. (2013) An old disk still capable of forming a planetary system. *Nature*493:644–646
- Bergin EA, Cleeves LI, Crockett N Blake GA (2014) Exploring the Origins of Carbon in Terrestrial Worlds. *Faraday Discussions* 168
- Bergin EA, Blake GA, Ciesla F, Hirschmann MM Li J (2015) Tracing the ingredients for a habitable earth from interstellar space through planet formation. *Proceedings of the National Academy of Science* 112:8965–8970
- Bitsch B, Crida A, Morbidelli A, Kley W Dobbs-Dixon I (2013) Stellar irradiated discs and implications on migration of embedded planets. I. Equilibrium discs. *A&A*549:A124
- Bitsch B, Lambrechts M Johansen A (2015) The growth of planets by pebble accretion in evolving protoplanetary discs. *A&A*582:A112
- Blandford RD Payne DG (1982) Hydromagnetic flows from accretion discs and the production of radio jets. *MNRAS*199:883–903
- Bodenheimer P Pollack JB (1986) Calculations of the accretion and evolution of giant planets The effects of solid cores. *Icarus*67:391–408
- Bolton SJ, Lunine J, Stevenson D et al. (2017) The Juno Mission. *Space Sci Rev*213:5–37
- Bond JC, O'Brien DP Laurotta DS (2010) The Compositional Diversity of Extrasolar Terrestrial Planets. I. In Situ Simulations. *ApJ*715:1050–1070
- Booth RA, Clarke CJ, Madhusudhan N Ilee JD (2017) Chemical enrichment of giant planets and discs due to pebble drift. *MNRAS*469:3994–4011
- Bosman AD, Bruderer S van Dishoeck EF (2017a) CO₂ infrared emission as a diagnostic of planet-forming regions of disks. *A&A*601:A36
- Bosman AD, Tielens AGGM van Dishoeck EF (2017b) Efficiency of radial transport of ices in protoplanetary disks probed with infrared observations: the case of CO₂. *ArXiv e-prints*
- Bowler BP (2016) Imaging Extrasolar Giant Planets. *PASP*128(10):102,001
- Brewer JM, Fischer DA Madhusudhan N (2017) C/O and O/H Ratios Suggest Some Hot Jupiters Originate Beyond the Snow Line. *AJ*153:83
- Brouwers MG, Vazan A Ormel CW (2017) How cores grow by pebble accretion I. Direct core growth. *ArXiv e-prints*
- Butscher T, Duvernay F, Theule P et al. (2015) Formation mechanism of glycolaldehyde and ethylene glycol in astrophysical ices from HCO and CH₂OH recombination: an experimental study. *MNRAS*453:1587–1596
- Chabrier G (2005) The Initial Mass Function: From Salpeter 1955 to 2005. In: Corbelli E, Palla F Zinnecker H (eds) *The Initial Mass Function 50 Years Later*, *Astrophysics and Space Science Library*, vol 327, p 41, DOI 10.1007/978-1-4020-3407-7_5
- Chabrier G Baraffe I (2007) Heat Transport in Giant (Exo)planets: A New Perspective. *ApJ*661:L81–L84
- Chambers JE (2009) An Analytic Model for the Evolution of a Viscous, Irradiated Disk. *ApJ*705:1206–1214

- Chatterjee S Ford EB (2015) Planetesimal Interactions Can Explain the Mysterious Period Ratios of Small Near-Resonant Planets. *ApJ*803:33
- Chatterjee S, Ford EB, Matsumura S Rasio FA (2008) Dynamical Outcomes of Planet-Planet Scattering. *ApJ*686:580-602
- Chen J Kipping D (2017) Probabilistic Forecasting of the Masses and Radii of Other Worlds. *ApJ*834:17
- Chiang E Laughlin G (2013) The minimum-mass extrasolar nebula: in situ formation of close-in super-Earths. *MNRAS*431:3444–3455
- Chiang EI Goldreich P (1997) Spectral Energy Distributions of T Tauri Stars with Passive Circumstellar Disks. *ApJ*490:368–376
- Chuang KJ, Fedoseev G, Qasim D et al. (2018) Reactive desorption of CO hydrogenation products under cold pre-stellar core conditions. *The Astrophysical Journal* 853(2):102, URL <http://stacks.iop.org/0004-637X/853/i=2/a=102>
- Cleeves LI, Adams FC Bergin EA (2013) Exclusion of Cosmic Rays in Protoplanetary Disks: Stellar and Magnetic Effects. *ApJ*772:5
- Cleeves LI, Bergin EA, Alexander CMO et al. (2014) The ancient heritage of water ice in the solar system. *Science* 345:1590–1593
- Coleman GAL Nelson RP (2014) On the formation of planetary systems via oligarchic growth in thermally evolving viscous discs. *MNRAS*445:479–499
- Coleman GAL Nelson RP (2016) Giant planet formation in radially structured protoplanetary discs. *MNRAS*460:2779–2795
- Cooper CS Showman AP (2006) Dynamics and Disequilibrium Carbon Chemistry in Hot Jupiter Atmospheres, with Application to HD 209458b. *ApJ*649:1048–1063
- Crida A Morbidelli A (2007) Cavity opening by a giant planet in a protoplanetary disc and effects on planetary migration. *MNRAS*377:1324–1336
- Cridland AJ, Pudritz RE Alessi M (2016) Composition of early planetary atmospheres - I. Connecting disc astrochemistry to the formation of planetary atmospheres. *MNRAS*461:3274–3295
- Cridland AJ, Pudritz RE Birnstiel T (2017a) Radial drift of dust in protoplanetary discs: the evolution of ice lines and dead zones. *MNRAS*465:3865–3878
- Cridland AJ, Pudritz RE, Birnstiel T, Cleeves LI Bergin EA (2017b) Composition of early planetary atmospheres - II. Coupled Dust and chemical evolution in protoplanetary discs. *MNRAS*469:3910–3927
- Cuzzi JN Zahnle KJ (2004) Material Enhancement in Protoplanetary Nebulae by Particle Drift through Evaporation Fronts. *ApJ*614:490–496
- Dittkrist KM, Mordasini C, Klahr H, Alibert Y Henning T (2014) Impacts of planet migration models on planetary populations. Effects of saturation, cooling and stellar irradiation. *A&A*567:A121
- Duffell PC, Haiman Z, MacFadyen AI, D’Orazio DJ Farris BD (2014) The Migration of Gap-opening Planets is Not Locked to Viscous Disk Evolution. *ApJ*792:L10
- Dutrey A, Guilloteau S Simon M (1994) Images of the GG Tauri rotating ring. *A&A*286:149–159
- Edgar RG (2008) Type II Migration: Varying Planet Mass and Disc Viscosity. *ArXiv e-prints*
- Eistrup C, Walsh C van Dishoeck EF (2016) Setting the volatile composition of (exo)planet-building material. Does chemical evolution in disk midplanes matter? *A&A*595:A83
- Elser S, Meyer MR Moore B (2012) On the origin of elemental abundances in the terrestrial planets. *Icarus*221:859–874
- Fabrycky D Tremaine S (2007) Shrinking Binary and Planetary Orbits by Kozai Cycles with Tidal Friction. *ApJ*669:1298–1315
- Fabrycky DC, Lissauer JJ, Ragozzine D et al. (2014) Architecture of Kepler’s Multi-transiting Systems. II. New Investigations with Twice as Many Candidates. *ApJ*790:146
- Fang J Margot JL (2012) Architecture of Planetary Systems Based on Kepler Data: Number of Planets and Coplanarity. *ApJ*761:92
- Fedele D, Bruderer S, van Dishoeck EF et al. (2013) Probing the Radial Temperature Structure of Protoplanetary Disks with Herschel/HIFI. *ApJ*776:L3
- Fischer DA Valenti J (2005) The Planet-Metallicity Correlation. *ApJ*622:1102–1117

- Flock M, Henning T Klahr H (2012) Turbulence in Weakly Ionized Protoplanetary Disks. *ApJ*761:95
- Fogel JKI, Bethell TJ, Bergin EA, Calvet N Semenov D (2011) Chemistry of a Protoplanetary Disk with Grain Settling and Ly α Radiation. *ApJ*726:29
- Frank A, Ray TP, Cabrit S et al. (2014) Jets and Outflows from Star to Cloud: Observations Confront Theory. *Protostars and Planets VI* pp 451–474
- Gammie CF (1996) Linear Theory of Magnetized, Viscous, Self-gravitating Gas Disks. *ApJ*462:725
- Gillett FC Forrest WJ (1973) Spectra of the Becklin-Neugebauer point source and the Kleinmann-Low nebula from 2.8 to 13.5 microns. *ApJ*179:483–491
- Goldreich P Tremaine S (1979) The excitation of density waves at the Lindblad and corotation resonances by an external potential. *ApJ*233:857–871
- González-Cataldo F, Wilson HF Militzer B (2014) Ab Initio Free Energy Calculations of the Solubility of Silica in Metallic Hydrogen and Application to Giant Planet Cores. *ApJ*787:79
- Gorti U, Liseau R, Sándor Z Clarke C (2016) Disk Dispersal: Theoretical Understanding and Observational Constraints. *Space Sci Rev*205:125–152
- Grasset O, Schneider J Sotin C (2009) A Study of the Accuracy of Mass-Radius Relationships for Silicate-Rich and Ice-Rich Planets up to 100 Earth Masses. *ApJ*693:722–733
- Gressel O, Turner NJ, Nelson RP McNally CP (2015) Global Simulations of Protoplanetary Disks With Ohmic Resistivity and Ambipolar Diffusion. *ApJ*801:84
- Haisch KE Jr, Lada EA Lada CJ (2001) Disk Frequencies and Lifetimes in Young Clusters. *ApJ*553:L153–L156
- Hansen BMS Murray N (2013) Testing in Situ Assembly with the Kepler Planet Candidate Sample. *ApJ*775:53
- Hartmann L (2008) Masses and mass distributions of protoplanetary disks. *Physica Scripta Volume T* 130(1):014012
- Hartmann L Kenyon SJ (1987) High spectral resolution infrared observations of V1057 Cygni. *ApJ*322:393–398
- Hasegawa Y (2016) Super-Earths as Failed Cores in Orbital Migration Traps. *ApJ*832:83
- Hasegawa Y Pudritz RE (2011) The origin of planetary system architectures - I. Multiple planet traps in gaseous discs. *MNRAS*417:1236–1259
- Hasegawa Y Pudritz RE (2013) Planetary Populations in the Mass-Period Diagram: A Statistical Treatment of Exoplanet Formation and the Role of Planet Traps. *ApJ*778:78
- Hasegawa Y Pudritz RE (2014) Planet Traps and Planetary Cores: Origins of the Planet-Metallicity Correlation. *ApJ*794:25
- Helled R, Bodenheimer P, Podolak M et al. (2014) Giant Planet Formation, Evolution, and Internal Structure. *Protostars and Planets VI* pp 643–665
- Helling C, Woitke P, Rimmer PB et al. (2014) Disk Evolution, Element Abundances and Cloud Properties of Young Gas Giant Planets. *Life* 4
- Henning T Semenov D (2013) Chemistry in Protoplanetary Disks. *Chemical Reviews* 113:9016–9042
- Hernández J, Calvet N, Briceño C et al. (2007) Spitzer Observations of the Orion OB1 Association: Disk Census in the Low-Mass Stars. *ApJ*671:1784–1799
- Howard AW, Marcy GW, Johnson JA et al. (2010) The Occurrence and Mass Distribution of Close-in Super-Earths, Neptunes, and Jupiters. *Science* 330:653
- Howard AW, Marcy GW, Bryson ST et al. (2012) Planet Occurrence within 0.25 AU of Solar-type Stars from Kepler. *ApJS*201:15
- Howard AW, Sanchis-Ojeda R, Marcy GW et al. (2013) A rocky composition for an Earth-sized exoplanet. *Nature*503:381–384
- Ida S Lin DNC (2004a) Toward a Deterministic Model of Planetary Formation. I. A Desert in the Mass and Semimajor Axis Distributions of Extrasolar Planets. *ApJ*604:388–413
- Ida S Lin DNC (2004b) Toward a Deterministic Model of Planetary Formation. II. The Formation and Retention of Gas Giant Planets around Stars with a Range of Metallicities. *ApJ*616:567–572

- Ida S Lin DNC (2005) Toward a Deterministic Model of Planetary Formation. III. Mass Distribution of Short-Period Planets around Stars of Various Masses. *ApJ*626:1045–1060
- Ida S Lin DNC (2008a) Toward a Deterministic Model of Planetary Formation. IV. Effects of Type I Migration. *ApJ*673:487–501
- Ida S Lin DNC (2008b) Toward a Deterministic Model of Planetary Formation. V. Accumulation Near the Ice Line and Super-Earths. *ApJ*685:584–595
- Ikoma M, Nakazawa K Emori H (2000) Formation of Giant Planets: Dependences on Core Accretion Rate and Grain Opacity. *ApJ*537:1013–1025
- Javoy M (1995) The integral enstatite chondrite model of the Earth. *Geophys Res Lett*22:2219–2222
- Johansen A, Oishi JS, Mac Low MM et al. (2007) Rapid planetesimal formation in turbulent circumstellar disks. *Nature*448:1022–1025
- Johnson JA, Aller KM, Howard AW Crepp JR (2010) Giant Planet Occurrence in the Stellar Mass-Metallicity Plane. *PASP*122:905
- Jørgensen JK, van Dishoeck EF, Visser R et al. (2009) PROSAC: a submillimeter array survey of low-mass protostars. II. The mass evolution of envelopes, disks, and stars from the Class 0 through I stages. *A&A*507:861–879
- Jørgensen JK, Favre C, Bisschop SE et al. (2012) Detection of the Simplest Sugar, Glycolaldehyde, in a Solar-type Protostar with ALMA. *ApJ*757:L4
- Jurić M Tremaine S (2008) Dynamical Origin of Extrasolar Planet Eccentricity Distribution. *ApJ*686:603–620
- Klassen M, Pudritz RE, Kuiper R, Peters T Banerjee R (2016) Simulating the Formation of Massive Protostars. I. Radiative Feedback and Accretion Disks. *ApJ*823:28
- Kley W Nelson RP (2012) Planet-Disk Interaction and Orbital Evolution. *ARA&A*50:211–249
- Kokubo E Ida S (2002) Formation of Protoplanet Systems and Diversity of Planetary Systems. *ApJ*581:666–680
- Kratter KM, Matzner CD Krumholz MR (2008) Global Models for the Evolution of Embedded, Accreting Protostellar Disks. *ApJ*681:375–390
- Krijt S Ciesla FJ (2016) Dust Diffusion and Settling in the Presence of Collisions: Trapping (sub)micron Grains in the Midplane. *ApJ*822:111
- Leconte J Chabrier G (2012) A new vision of giant planet interiors: Impact of double diffusive convection. *A&A*540:A20
- Leconte J Chabrier G (2013) Layered convection as the origin of Saturn’s luminosity anomaly. *Nature Geoscience* 6:347–350
- Lesur G, Kunz MW Fromang S (2014) Thanatology in protoplanetary discs. The combined influence of Ohmic, Hall, and ambipolar diffusion on dead zones. *A&A*566:A56
- Li ZY, Banerjee R, Pudritz RE et al. (2014) The Earliest Stages of Star and Planet Formation: Core Collapse, and the Formation of Disks and Outflows. *Protostars and Planets VI* pp 173–194
- Ligterink NFW, Coutens A, Kofman V et al. (2017) The ALMA-PILS survey: detection of CH₃NCO towards the low-mass protostar IRAS 16293-2422 and laboratory constraints on its formation. *MNRAS*469:2219–2229
- Lin DNC Papaloizou J (1986) On the tidal interaction between protoplanets and the primordial solar nebula. II - Self-consistent nonlinear interaction. *ApJ*307:395–409
- Lin DNC Papaloizou JCB (1993) On the tidal interaction between protostellar disks and companions. In: Levy EH Lunine JI (eds) *Protostars and Planets III*, pp 749–835
- Lissauer JJ, Ragozzine D, Fabrycky DC et al. (2011) Architecture and Dynamics of Kepler’s Candidate Multiple Transiting Planet Systems. *ApJS*197:8
- Lozovsky M, Helled R, Rosenberg ED Bodenheimer P (2017) Jupiter’s Formation and Its Primordial Internal Structure. *ApJ*836:227
- Lynden-Bell D Pringle JE (1974) The evolution of viscous discs and the origin of the nebular variables. *MNRAS*168:603–637
- Lyra W, Paardekooper SJ Mac Low MM (2010) Orbital Migration of Low-mass Planets in Evolutionary Radiative Models: Avoiding Catastrophic Infall. *ApJ*715:L68–L73

- Madhusudhan N, Amin MA Kennedy GM (2014) Toward Chemical Constraints on Hot Jupiter Migration. *ApJ*794:L12
- Madhusudhan N, Bitsch B, Johansen A Eriksson L (2017) Atmospheric signatures of giant exoplanet formation by pebble accretion. *MNRAS*469:4102–4115
- Mayor M Queloz D (1995) A Jupiter-mass companion to a solar-type star. *Nature*378:355–359
- McClure MK, Bergin EA, Cleaves LI et al. (2016) Mass Measurements in Protoplanetary Disks from Hydrogen Deuteride. *ApJ*831:167
- McNally CP, Nelson RP, Paardekooper SJ, Gressel O Lyra W (2017) Low mass planet migration in magnetically torqued dead zones - I. Static migration torque. *MNRAS*472:1565–1575
- Militzer B Hubbard WB (2013) An Initial Equation of State for Hydrogen-Helium Mixtures with Recalibration of the Giant-planet Mass-Radius Relation. *ApJ*774:148
- Miyake K Nakagawa Y (1993) Effects of particle size distribution on opacity curves of protoplanetary disks around T Tauri stars. *Icarus*106:20
- Mizuno H, Nakazawa K Hayashi C (1978) Instability of a gaseous envelope surrounding a planetary core and formation of giant planets. *Progress of Theoretical Physics* 60:699–710
- Mollière P, van Boekel R, Bouwman J et al. (2017) Observing transiting planets with JWST. Prime targets and their synthetic spectral observations. *A&A*600:A10
- Mordasini C, Klahr H, Alibert Y, Miller N Henning T (2014) Grain opacity and the bulk composition of extrasolar planets. I. Results from scaling the ISM opacity. *A&A*566:A141
- Mordasini C, van Boekel R, Mollière P, Henning T Benneke B (2016) The Imprint of Exoplanet Formation History on Observable Present-day Spectra of Hot Jupiters. *ApJ*832:41
- Moriarty J, Madhusudhan N Fischer D (2014) Chemistry in an Evolving Protoplanetary Disk: Effects on Terrestrial Planet Composition. *ApJ*787:81
- Öberg KI, Boogert ACA, Pontoppidan KM et al. (2011a) The Spitzer Ice Legacy: Ice Evolution from Cores to Protostars. *ApJ*740:109
- Öberg KI, Murray-Clay R Bergin EA (2011b) The Effects of Snowlines on C/O in Planetary Atmospheres. *ApJ*743:L16
- Ormel CW, Paszun D, Dominik C Tielens AGGM (2009) Dust coagulation and fragmentation in molecular clouds. I. How collisions between dust aggregates alter the dust size distribution. *A&A*502:845–869
- Owen JE, Ercolano B Clarke CJ (2011) Protoplanetary disc evolution and dispersal: the implications of X-ray photoevaporation. *MNRAS*412:13–25
- Paardekooper SJ, Baruteau C, Cridland A Kley W (2010) A torque formula for non-isothermal type I planetary migration - I. Unsaturated horseshoe drag. *MNRAS*401:1950–1964
- Papaloizou J Lin DNC (1984) On the tidal interaction between protoplanets and the primordial solar nebula. I - Linear calculation of the role of angular momentum exchange. *ApJ*285:818–834
- Pascucci I Sterzik M (2009) Evidence for Disk Photoevaporation Driven by the Central Star. *ApJ*702:724–732
- Pasek MA, Milsom JA, Ciesla FJ et al. (2005) Sulfur chemistry with time-varying oxygen abundance during Solar System formation. *Icarus*175:1–14
- Pelletier G Pudritz RE (1992) Hydromagnetic disk winds in young stellar objects and active galactic nuclei. *ApJ*394:117–138
- Pepe F, Mayor M, Queloz D et al. (2004) The HARPS search for southern extra-solar planets. I. HD 330075 b: A new “hot Jupiter”. *A&A*423:385–389
- Pignatale FC, Maddison ST, Taquet V, Brooks G Liffman K (2011) The effect of the regular solution model in the condensation of protoplanetary dust. *MNRAS*414:2386–2405
- Pinhas A, Madhusudhan N Clarke C (2016) Efficiency of planetesimal ablation in giant planetary envelopes. *MNRAS*463:4516–4532
- Pollack JB, Hubickyj O, Bodenheimer P et al. (1996) Formation of the Giant Planets by Concurrent Accretion of Solids and Gas. *Icarus*124:62–85
- Pontoppidan KM, Salyk C, Bergin EA et al. (2014) Volatiles in Protoplanetary Disks. *Protostars and Planets VI* pp 363–385

- Pudritz RE Norman CA (1986) Bipolar hydromagnetic winds from disks around protostellar objects. *ApJ*301:571–586
- Pudritz RE, Ouyed R, Fendt C Brandenburg A (2007) Disk Winds, Jets, and Outflows: Theoretical and Computational Foundations. *Protostars and Planets V* pp 277–294
- Qi C, Öberg KI, Wilner DJ et al. (2013) Imaging of the CO Snow Line in a Solar Nebula Analog. *Science* 341:630–632
- Queiroz D, Mayor M, Weber L et al. (2000) The CORALIE survey for southern extra-solar planets. I. A planet orbiting the star Gliese 86. *A&A*354:99–102
- Raettig N, Klahr H Lyra W (2015) Particle Trapping and Streaming Instability in Vortices in Protoplanetary Disks. *ApJ*804:35
- Ray T, Dougados C, Bacciotti F, Eisloffel J Chrysostomou A (2007) Toward Resolving the Outflow Engine: An Observational Perspective. *Protostars and Planets V* pp 231–244
- Raymond SN, Kokubo E, Morbidelli A, Morishima R Walsh KJ (2014) Terrestrial Planet Formation at Home and Abroad. *Protostars and Planets VI* pp 595–618
- Rivilla VM, Beltrán MT, Cesaroni R et al. (2017) Formation of ethylene glycol and other complex organic molecules in star-forming regions. *A&A*598:A59
- Rogers LA (2014) Glimpsing the Compositions of Sub-Neptune-Size Exoplanets. In: Booth M, Matthews BC Graham JR (eds) *Exploring the Formation and Evolution of Planetary Systems*, IAU Symposium, vol 299, pp 247–251, DOI 10.1017/S1743921313008491
- Ros K Johansen A (2013) Ice condensation as a planet formation mechanism. *A&A*552:A137
- Ruden SP (2004) Evolution of Photoevaporating Protoplanetary Disks. *ApJ*605:880–891
- Salmeron R Wardle M (2003) Magnetorotational instability in stratified, weakly ionized accretion discs. *MNRAS*345:992–1008
- Salyk C, Pontoppidan KM, Blake GA et al. (2008) H₂O and OH Gas in the Terrestrial Planet-forming Zones of Protoplanetary Disks. *ApJ*676:L49
- Schäfer U, Yang CC Johansen A (2017) Initial mass function of planetesimals formed by the streaming instability. *A&A*597:A69
- Seifried D, Banerjee R, Pudritz RE Klessen RS (2015) Accretion and magnetic field morphology around Class 0 stage protostellar discs. *MNRAS*446:2776–2788
- Shakura NI Sunyaev RA (1973) Black holes in binary systems. Observational appearance. *A&A*24:337–355
- Showman AP Guillot T (2002) Atmospheric circulation and tides of “51 Pegasus b-like” planets. *A&A*385:166–180
- Simon JB, Armitage PJ, Li R Youdin AN (2016) The Mass and Size Distribution of Planetesimals Formed by the Streaming Instability. I. The Role of Self-gravity. *ApJ*822:55
- Spezzano S, Caselli P, Bizzocchi L, Giuliano BM Lattanzi V (2017) The observed chemical structure of L1544. *A&A*606:A82
- Stammler SM, Birnstiel T, Panić O, Dullemond CP Dominik C (2017) Redistribution of CO at the location of the CO ice line in evolving gas and dust disks. *A&A*600:A140
- Stevenson DJ (1985) Cosmochemistry and structure of the giant planets and their satellites. *Icarus*62:4–15
- Stevenson DJ Lunine JI (1988) Rapid formation of Jupiter by diffuse redistribution of water vapor in the solar nebula. *Icarus*75:146–155
- Tamayo D, Triaud AHMJ, Menou K Rein H (2015) Dynamical Stability of Imaged Planetary Systems in Formation: Application to HL Tau. *ApJ*805:100
- Terquem C Papaloizou JCB (1996) On the stability of an accretion disc containing a toroidal magnetic field. *MNRAS*279:767–784
- Testi L, Birnstiel T, Ricci L et al. (2014) Dust Evolution in Protoplanetary Disks. *Protostars and Planets VI* pp 339–361
- Thiabaud A, Marboeuf U, Alibert Y, Leya I Mezger K (2015) Gas composition of the main volatile elements in protoplanetary discs and its implication for planet formation. *A&A*574:A138
- Tobin JJ, Looney LW, Wilner DJ et al. (2015) A Sub-arcsecond Survey Toward Class 0 Protostars in Perseus: Searching for Signatures of Protostellar Disks. *ApJ*805:125

- Toppani A, Libourel G, Robert F Ghanbaja J (2006) Laboratory condensation of refractory dust in protosolar and circumstellar conditions. *Geochim Cosmochim Acta*70:5035–5060
- Turner NJ, Fromang S, Gammie C et al. (2014) Transport and Accretion in Planet-Forming Disks. *Protostars and Planets VI* pp 411–432
- Udry S Santos NC (2007) Statistical Properties of Exoplanets. *ARA&A*45:397–439
- Umebayashi T Nakano T (2009) Effects of Radionuclides on the Ionization State of Protoplanetary Disks and Dense Cloud Cores. *ApJ*690:69–81
- Valencia D, Sasselov DD O’Connell RJ (2007) Detailed Models of Super-Earths: How Well Can We Infer Bulk Properties? *ApJ*665:1413–1420
- Vasyunin AI, Caselli P, Dulieu F Jiménez-Serra I (2017) Formation of Complex Molecules in Prestellar Cores: A Multilayer Approach. *ApJ*842:33
- Wahl SM, Hubbard WB, Militzer B et al. (2017) Comparing Jupiter interior structure models to Juno gravity measurements and the role of a dilute core. *Geophys Res Lett*44:4649–4659
- Walsh C, Millar TJ, Nomura H et al. (2014) Complex organic molecules in protoplanetary disks. *A&A*563:A33
- Walsh C, Nomura H van Dishoeck E (2015) The molecular composition of the planet-forming regions of protoplanetary disks across the luminosity regime. *A&A*582:A88
- Wang J Fischer DA (2015) Revealing a Universal Planet-Metallicity Correlation for Planets of Different Sizes Around Solar-type Stars. *AJ*149:14
- Ward WR (1986) Density waves in the solar nebula - Differential Lindblad torque. *Icarus*67:164–180
- Ward WR (1997) Protoplanet Migration by Nebula Tides. *Icarus*126:261–281
- Weidenschilling SJ (1977) Aerodynamics of solid bodies in the solar nebula. *MNRAS*180:57–70
- Weiss LM, Marcy GW, Rowe JF et al. (2013) The Mass of KOI-94d and a Relation for Planet Radius, Mass, and Incident Flux. *ApJ*768:14
- Xu R, Bai XN Öberg K (2017) Turbulent-diffusion Mediated CO Depletion in Weakly Turbulent Protoplanetary Disks. *ApJ*835:162
- Yan H Lazarian A (2002) Scattering of Cosmic Rays by Magnetohydrodynamic Interstellar Turbulence. *Physical Review Letters* 89:281102
- Youdin AN Goodman J (2005) Streaming Instabilities in Protoplanetary Disks. *ApJ*620:459–469
- Youdin AN Shu FH (2002) Planetesimal Formation by Gravitational Instability. *ApJ*580:494–505
- Yu L, Donati JF, Hébrard EM et al. (2017) A hot Jupiter around the very active weak-line T Tauri star TAP 26. *MNRAS*467:1342–1359
- Yu M, Willacy K, Dodson-Robinson SE, Turner NJ Evans NJ II (2016) Probing Planet Forming Zones with Rare CO Isotopologues. *ApJ*822:53
- Zapolsky HS Salpeter EE (1969) The Mass-Radius Relation for Cold Spheres of Low Mass. *ApJ*158:809
- Zhang K, Blake GA Bergin EA (2015) Evidence of Fast Pebble Growth Near Condensation Fronts in the HL Tau Protoplanetary Disk. *ApJ*806:L7